J|A|C|S ARTICLES

Published on Web 01/15/2009

Synthesis, Structural Characterization, and Unusual Field-Effect Behavior of Organic Transistor Semiconductor Oligomers: Inferiority of Oxadiazole Compared with Other Electron-Withdrawing Subunits

Taegweon Lee,† Chad A. Landis,† Bal Mukund Dhar,† Byung Jun Jung,† Jia Sun,† Amy Sarjeant,† Ho-Jin Lee,‡ and Howard E. Katz*,†

Department of Materials Science and Engineering and Department of Chemistry, Johns Hopkins University, 3400 North Charles Street, Baltimore, Maryland 21218, and Department of Structural Biology, St. Jude Children's Research Hospital, Memphis, Tennessee 38105

Received September 11, 2008; E-mail: hekatz@jhu.edu

Abstract: A new series of heterocyclic oligomers based on the 1,3,4-oxadiazole ring were synthesized. Other electron-deficient cores (fluorenone and fumaronitrile) were introduced to investigate the oligomers as n-channel materials. The physical properties, thin film morphologies, and field-effect transistor characteristics of the oligomers were evaluated. Thin films were deposited at different substrate temperatures and on variously coated Si/SiO_2 for device optimization. Contrary to our expectations, the thin film devices of **4** revealed p-channel behavior, and the average hole mobility was 0.14 $cm^2\ V^{-1}\ s^{-1}$ (maximum value 0.18 $cm^2\ V^{-1}\ s^{-1}$). Compound **11** is the first example of an oxadiazole-containing organic semiconductor (OSC) oligomer in an n-channel organic field-effect transistor (OFET) and shows moderate mobilities. Non-oxadiazole-containing oligomers **9** and **12** showed n-channel OFET behavior on hexamethyldisilazane-treated and Cytop spin-coated SiO_2 in vacuum. These are the first fluorenone- and fumaronitrile-based n-OSCs demonstrated in transistors. However, oxadiazole-core materials **14** and **16** were inactive in transistor devices.

Introduction

Organic semiconductors (OSCs) have attracted great attention because of potential applications that include flexible active circuits,[1] transducers and displays comprising organic light-emitting diodes (OLEDs),[2] organic field-effect transistors (OFETs),[3] organic photovoltaics (OPVs),[4] organic diodes,[5] and organic memory.[6] Organic electronic materials can be employed in specialized niche markets because of their advantages of low cost, easy manufacture (low-temperature fabrication and solution processing), printability, and large-area processing on flexible plastics. After over a decade of vigorous research, OFETs have been extensively developed. Since the pioneering demonstrations of organic transistors were reported by the Ando and Garnier groups,[7] OFETs have come to show predictable performance, including mobility (>0.1 $cm^2\ V^{-1}\ s^{-1}$) and on/off ratio (10^6) equivalent to those of amorphous silicon devices,[8] and are being introduced into technologies such as chemical sensors[9] and radio-frequency identification (RFID) tags.[10] Hole-carrying (p-channel) organic semiconductors (p-OSCs), comprising rela-

† Johns Hopkins University.
‡ St. Jude Children's Research Hospital.

(1) (a) Jackson, T. N. *Nat. Mater.* **2005**, *4*, 581. (b) Gundlach, D. J. *Nat. Mater.* **2007**, *6*, 173. (c) Kelley, T. W.; Baude, P. F.; Gerlach, C.; Ender, D. E.; Muyres, D.; Haase, M. A.; Vogel, D. E.; Theiss, S. D. *Chem. Mater.* **2004**, *16*, 4413.
(2) (a) Tang, C. W.; Vanslyke, S. A. *Appl. Phys. Lett.* **1987**, *51*, 913. (b) Hide, F.; Díaz-García, M. A.; Schwartz, B. J.; Heeger, A. J. *Acc. Chem. Res.* **1997**, *30*, 430.
(3) (a) Garnier, F.; Hajlaoui, R.; Yassar, A.; Shirakawa, P. *Science* **1994**, *265*, 1684. (b) Muccini, M. *Nat. Mater.* **2006**, *5*, 605. (c) Murphy, A. R.; Fréchet, J. M. J. *Chem. Rev.* **2007**, *107*, 1066.
(4) (a) Brabec, C. J.; Sariciftci, N. S.; Hummelen, J. C. *Adv. Funct. Mater.* **2001**, *11*, 15. (b) Peumans, P.; Yakimov, A.; Forrest, S. R. *J. Appl. Phys.* **2003**, *93*, 3693. (c) Günes, S.; Neugebauer, H.; Sariciftci, N. S. *Chem. Rev.* **2007**, *107*, 1324. (d) Kim, J. Y.; Lee, K.; Coates, N. E.; Moses, D.; Nguyen, T.-Q.; Dante, M.; Heeger, A. J. *Science* **2007**, *317*, 222. (e) Thompson, B. C.; Fréchet, J. M. J. *Angew. Chem., Int. Ed.* **2008**, *47*, 58.
(5) (a) Roman, L. S.; Inganas, M. O. *Appl. Phys. Lett.* **1999**, *75*, 3557. (b) Chen, K. M.; Zhang, Y. X.; Qin, G. G.; Jin, S. X.; Wu, K.; Li, C. Y.; Gu, Z. N.; Zhou, X. H. *Appl. Phys. Lett.* **1996**, *69*, 3557.
(6) (a) Ma, L.; Pyo, S.; Ouyang, J.; Xu, Q.; Yang, Y. *Appl. Phys. Lett.* **2003**, *82*, 1419. (b) Tour, J. M.; Cheng, L.; Nackashi, D. P.; Yao, Y.; Flatt, A. K.; St. Angelo, S. K.; Mallouk, T. E.; Franzon, P. D. *J. Am. Chem. Soc.* **2003**, *125*, 13279. (c) Seo, K.; Konchenko, A. V.; Lee, J.; Bang, G. S.; Lee, H. *J. Am. Chem. Soc.* **2008**, *130*, 2553.
(7) (a) Tsumura, A.; Koezuka, H.; Ando, T. *Appl. Phys. Lett.* **1986**, *49*, 1210. (b) Fichou, D.; Horowitz, G.; Nishikitani, Y.; Roncali, J.; Garnier, F. *Synth. Met.* **1989**, *28*, C729. (c) Horowitz, G.; Fichou, D.; Peng, X. Z.; Garnier, F. *Synth. Met.* **1991**, *41*, 1127. (d) Garnier, F.; Horowitz, G.; Peng, X. Z.; Fichou, D. *Synth. Met.* **1991**, *45*, 163.
(8) (a) Payne, M. M.; Parkin, S. R.; Anthony, J. E.; Kuo, C.-C.; Jackson, T. N. *J. Am. Chem. Soc.* **2005**, *127*, 4986. (b) Takimiya, K.; Ebata, H.; Sakamoto, K.; Izawa, T.; Otsubo, T.; Kunugi, Y. *J. Am. Chem. Soc.* **2006**, *128*, 12604. (c) Yamamoto, T.; Takimiya, K. *J. Am. Chem. Soc.* **2007**, *129*, 2224. (d) Ebata, H.; Izawa, T.; Miyazaki, E.; Takimiya, K.; Ikeda, M.; Kuwabara, H.; Yui, T. *J. Am. Chem. Soc.* **2007**, *129*, 15732.
(9) (a) Zhu, Z. T.; Mason, J. T.; Dieckmann, R.; Malliaras, G. G. *Appl. Phys. Lett.* **2002**, *81*, 4643. (b) Crone, B. K.; Dodabalapur, A.; Sarpeshkar, R.; Gelperin, A.; Katz, H. E.; Bao, Z. *J. Appl. Phys.* **2002**, *91*, 10140. (c) See, K. C.; Becknell, A.; Miragliotta, J.; Katz, H. E. *Adv. Mater.* **2007**, *19*, 3322. (d) Huang, J.; Miragliotta, J.; Becknell, A.; Katz, H. E. *J. Am. Chem. Soc.* **2007**, *129*, 9366. (e) Huang, J.; Sun, J.; Katz, H. E. *Adv. Mater.* **2008**, *20*, 2567.

10.1021/ja807219x CCC: $40.75

tively electron-rich conjugated π systems, are studied most often, and there are now dozens of examples that meet the amorphous silicon benchmarks, including pentacene, which has been used in commercial display backplane prototypes.[11] There are considerably fewer electron-carrying (n-channel) organic semiconductors (n-OSCs),[12] though their numbers have increased over the last two years. The development of n-OSCs is important for the realization of organic p−n junctions, bipolar transistors, and complementary integrated circuits composed of both p- and n-OSCs.[13] The limitation on n-OSCs is that electrons are generally much less stable on organic semiconductors than are holes. During transport, electrons are easily quenched by environmental oxidation sources such as oxygen and water. Therefore, the chemical restrictions on air-stable n-OSCs are increased relative to p-OSCs. There are a few examples of air-stable n-OSCs, most of which have highly electron-withdrawing groups as part the conjugated systems, such as naphthalene and perylene tetracarboxylic diimides (NTCDI and PTCDI, respectively) with perfluoroalkyl side chains[14] or cyano-substitutued aromatic species.[15] These electron-withdrawing groups lower the energies of the lowest unoccupied molecular orbitals, so electrons injected or transported therein are stabilized against the environment.

To further the development of n-OSCs, we considered 1,3,4-oxadiazole as an attractive subunit because it would be expected to maintain the planarity and conjugation of an oligomer while having a higher electron affinity than other heterocycles. Oxadiazole derivatives have been widely used in bioorganic and medicinal chemistry[16] and as the electron-transporting[17] and hole-blocking materials[18] for OLEDs, both as small molecules and in polymers. Despite their wide use in OLEDs, there was no published successful attempt to use oxadiazole oligomers as parts of OSCs in transistors before our own report of a p-channel OFET.[19a] This surprising result prompted us to introduce additional electron-withdrawing segments, such as fluorenone and diphenylfumaronitrile, along with perfluorinated end groups into oxadiazole-containing oligomers in order to see how much additional electron-withdrawing power would be needed for oxadiazoles to be applicable as conjugated systems for n-OSCs or whether they would be useful at all. Interestingly, even in the case of the electron-deficient fluorenone ring, only a few material derivatives have been reported as OSCs, and they have been reported in p-channel OFETs by Porzio et al.[20] Fumaronitrile derivatives have recently been applied to non-doped red OLEDs[21] and organic nanoparticles.[22] Despite their strong electron-accepting ability, there has been no attempt to fabricate n-channel OFETs with fumaronitrile cores, though tricyanovinyl and dicyanomethylene n-OSCs have been demonstrated.[23]

In this paper, we describe the synthesis and characterization of two new bromothienyl oxadiazole intermediates with perfluoroalkyl end moieties, seven new oxadiazole-based conjugated oligomers as OSC candidates, and two non-oxadiazole-containing OSCs for comparison. We introduce the electron-deficient segments fluorenone and fumaronitrile, in addition to the oxadiazole ring, to the library of conjugated OSC segments. We morphologically and electrically characterize these compounds as solid thin films. Most of the oxadiazole-based organic semiconductors did not show any transistor behavior; the exceptions were **4** (p-channel) and **11** (n-channel, the first such example reported). Two comparative oligomers without the oxadiazole rings (**9** and **12**) showed n-channel OFET activity, demonstrating the utility of the fluorenone and fumaronitrile segments. Thus, despite the long history of using oxadiazoles

(10) (a) Voss, D. *Nature* **2000**, *407*, 442. (b) Baude, P. F.; Ender, D. A.; Haase, M. A.; Kelley, T. W.; Muyres, D. V.; Thesis, S. D. *Appl. Phys. Lett.* **2003**, *82*, 3964. (c) Cantatore, E.; Geuns, T. C. T.; Gelinck, G. H.; van Veenendaal, E.; Gruijthuijsen, A. F. A.; Schrijnemakers, L.; Drews, S.; de Leeuw, D. M. *IEEE J. Solid-State Circuits* **2007**, *42*, 84.

(11) (a) Gelinck, G. H.; et al. *Nat. Mater.* **2004**, *3*, 106. (b) Zhou, L.; Wanga, A.; Wu, S.-C.; Sun, J.; Park, S.; Jackson, T. N. *Appl. Phys. Lett.* **2006**, *88*, 083502.

(12) (a) Ando, S.; Murakami, R.; Nishida, J.-I.; Tada, H.; Inoue, Y.; Tokito, S.; Yamashita, Y. *J. Am. Chem. Soc.* **2005**, *127*, 14996. (b) Dimitrakopoulos, C. D.; Malenfant, P. R. L. *Adv. Mater.* **2002**, *14*, 99. (c) Newman, C. R.; Frisbie, C. D.; da Silva Filho, D. A.; Bredas, J. L.; Ewbank, P. C.; Mann, K. R. *Chem. Mater.* **2004**, *16*, 4436. (d) Facchetti, A.; Mushrush, M.; Yoon, M.-H.; Hutchison, G. R.; Ratner, M. A.; Marks, T. J. *J. Am. Chem. Soc.* **2004**, *126*, 13859. (e) Facchetti, A.; Yoon, M.-H.; Stern, C. L.; Hutchison, G. R.; Ratner, M. *J. Am. Chem. Soc.* **2004**, *126*, 13480. (f) Ie, Y.; Nitani, M.; Ishikawa, M.; Nakayama, K.; Tada, H.; Kaneda, T.; Aso, Y. *Org. Lett.* **2007**, *9*, 2115.

(13) (a) Yu, G.; Gao, J. J.; Hummelen, C.; Wudl, F.; Heeger, A. J. *Science* **1995**, *270*, 1789. (b) Katz, H. E.; Otsuki, J.; Yamazaki, K.; Suka, A.; Takido, T.; Lovinger, A. J.; Raghavachari, K. *Chem. Lett.* **2003**, *32*, 508. (c) Chesterfield, R. J.; Newman, C. R.; Pappenfus, T. M.; Ewbank, P. C.; Haukaas, M. H.; Mann, K. R.; Miller, L. L.; Frisbie, C. D. *Adv. Mater.* **2003**, *15*, 1278. (d) Crone, B.; Dodabalapur, A.; Lin, Y. Y.; Filas, R. W.; Bao, Z.; LaDuca, A.; Sarpeshkar, R.; Katz, H. E.; Li, W. *Nature* **2000**, *403*, 521. (e) Heidenhain, S. B.; Sakamoto, Y.; Suzuki, T.; Miura, A.; Fujikawa, H.; Mori, T.; Tokito, S.; Taga, Y. *J. Am. Chem. Soc.* **2000**, *122*, 10240.

(14) (a) Katz, H. E.; Lovinger, A. J.; Johnson, J.; Kloc, C.; Siegrist, T.; Li, W.; Lin, Y.-Y.; Dodabalapur, A. *Nature* **2000**, *404*, 478. (b) Katz, H. E.; Johnson, J.; Lovinger, A. J.; Li, W. *J. Am. Chem. Soc.* **2000**, *122*, 7787. (c) Weitz, R. T.; Amsharov, K.; Zschieschang, U.; Villas, E. B.; Goswami, D. K.; Burghard, M.; Dosch, H.; Jansen, M.; Kern, K.; Klauk, H. *J. Am. Chem. Soc.* **2008**, *130*, 4637. (d) See, K. C.; Landis, C.; Sarjeant, A.; Katz, H. E. *Chem. Mater.* **2008**, *20*, 3609. (e) Schmidt, R.; Ling, M. M.; Oh, J. H.; Winkler, M.; Könemann, M.; Bao, Z.; Würthner, F. *Adv. Mater.* **2007**, *19*, 3692. (f) Hosoi, Y.; Tsunami, D.; Ishii, H.; Furukawa, Y. *Chem. Phys. Lett.* **2007**, *436*, 139. (g) Chen, H. Z.; Ling, M. M.; Mo, X.; Shi, M. M.; Wang, M.; Bao, Z. *Chem. Mater.* **2007**, *19*, 816.

(15) (a) Usta, H.; Facchetti, A.; Marks, T. J. *J. Am. Chem. Soc.* **2008**, *130*, 8580. (b) Usta, H.; Facchetti, A.; Marks, T. J. *Org. Lett.* **2008**, *10*, 1385. (c) Jones, B. A.; Facchetti, A.; Marks, T. J.; Wasielewski, M. R. *Chem. Mater.* **2007**, *19*, 2703.

(16) (a) Narayanaa, B.; Raja, K. K. V.; Ashalathaa, B. V.; Kumarib, N. S. *Arch. Pharm. Chem. Life Sci.* **2005**, *338*, 373. (b) Romine, J. L.; Martin, S. W.; Meanwell, N. A.; Gribkoff, V. K.; Boissard, C. G.; Dworetzky, S. I.; Natale, J.; Moon, S.; Ortiz, A.; Yeleswaram, S.; Pajor, L.; Gao, Q.; Starrett, J. E., Jr *J. Med. Chem.* **2007**, *50*, 528.

(17) (a) Adachi, C.; Tsutsui, T.; Saito, S. *Appl. Phys. Lett.* **1990**, *56*, 799. (b) Risko, C.; Zojer, E.; Brocorens, P.; Marder, S. R.; Bredas, J. L. *Chem. Phys.* **2005**, *313*, 151. (c) Janietz, S.; Anlauf, S.; Wedel, A. *Macromol. Chem. Phys.* **2002**, *203*, 433. (d) Zhan, X.; Liu, Y.; Wu, X.; Wang, S.; Zhu, D. *Macromolecules* **2002**, *35*, 2529.

(18) Zhao, P.; Zhu, X.; Chen, J.; Ma, D.; Huang, W. *Synth. Met.* **2006**, *156*, 763.

(19) (a) Landis, C. A.; Dhar, B. M.; Lee, T.; Sarjeant, A.; Katz, H. E. *J. Phys. Chem. C* **2008**, *112*, 7939. (b) Ono, K.; Wakida, M.; Hosokawa, R.; Saito, K.; Nishida, J.; Yamashita, Y. *Heterocycles* **2007**, *72*, 85.

(20) (a) Porzio, W.; Destri, S.; Giovanella, U.; Pasini, M.; Motta, T.; Natali, D.; Sampietro, M.; Campione, M. *Thin Solid Films* **2005**, *492*, 212. (b) Porzio, W.; Destri, S.; Pasini, M.; Giovanella, U.; Motta, T.; Iosip, M. D.; Natali, D.; Sampietro, M.; Francoc, L.; Campione, M. *Synth. Met.* **2004**, *146*, 259.

(21) (a) Yeh, H.-C.; Yeh, S.-J.; Chen, C.-T. *Chem. Commun.* **2003**, 2632. (b) Yeh, H.-C.; Chan, L.-H.; Wua, W.-C.; Chen, C.-T. *J. Mater. Chem.* **2004**, *14*, 1293.

(22) Palayangoda, S. S.; Cai, X.; Adhikari, R. M.; Neckers, D. C. *Org. Lett.* **2008**, *10*, 281.

(23) (a) Cai, X.; Burand, M. W.; Newman, C. R.; da Silva Filho, D. A.; Pappenfus, T. M.; Bader, M. M.; Brédas, J.-L.; Mann, K. R.; Frisbie, C. D. *J. Phys. Chem. B* **2006**, *110*, 14590. (b) Chesterfield, R. J.; Newman, C. R.; Pappenfus, T. M.; Ewbank, P. C.; Haukaas, M. H.; Mann, K. R.; Miller, L. L.; Frisbie, C. D. *Adv. Mater.* **2003**, *15*, 1278. (c) Pappenfus, T. M.; Chesterfield, R. J.; Frisbie, C. D.; Mann, K. R.; Casado, J.; Raff, J. D.; Miller, L. L. *J. Am. Chem. Soc.* **2002**, *124*, 4184. (d) Handa, S.; Miyazaki, E.; Takimiya, K.; Kunugi, Y. *J. Am. Chem. Soc.* **2007**, *129*, 11684.

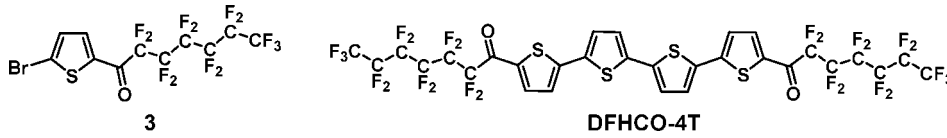

Figure 1. Chemical structures of **3** and **DFHCO-4T**.

Scheme 1. Synthetic Routes to Perfluoro-Ended Bromooxadiazoles **1** and **2**

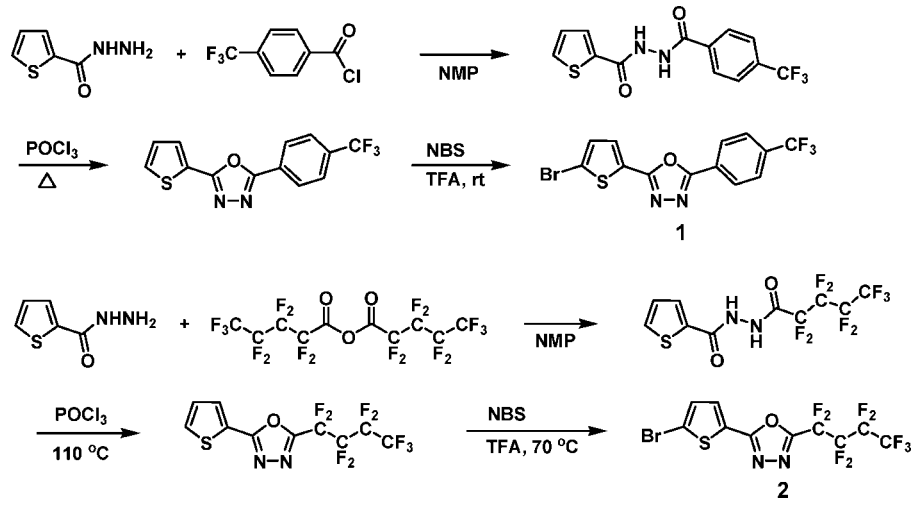

Scheme 2. Synthesis of Oxadiazole−Quaterthiophene Oligomer **4**

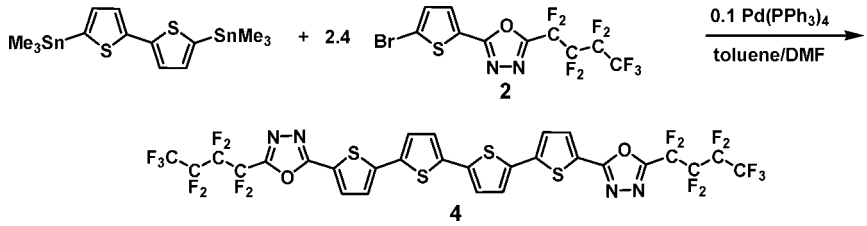

at the electron-injecting side of OLEDs and their favorable reduction potentials, they appear to have an unexpectedly deleterious effect in OFETs.

Results and Discussion

Synthesis. Scheme 1 illustrates the synthetic procedures for bromothiophene compounds containing electron-deficient oxadiazole and perfluoroalkyl end groups, the latter having been shown to be particularly useful for n-OSCs. 2-(5-Bromo-2-thienyl)-5-(4-trifluoromethylphenyl)-1,3,4-oxadiazole (**1**) was synthesized by the same procedure described in previous papers.[19] The bromination with *N*-bromosuccinimide (NBS) to form **1** was performed successfully at room temperature in a 3:1 CF_3COOH/dichloromethane mixed solvent instead of the more commonly used solvents, such as dimethylformamide (DMF) or a $CHCl_3/CH_3COOH$ mixture.[24] To realize more electron-deficient end functionality, we directly attached a terminal perfluorobutyl group to the oxadiazole. The carbonyl of perfluoropentanoic anhydride was easily nucleophilically attacked by 2-thiophenecarboxylic acid hydrazide in *N*-methylpyrrolidone (NMP), forming *N*-(perfluoropentanoyl)-*N*′-(2-thiophenecarbonyl)hydrazide along with perfluoropentanoic acid as a side product. The oxadiazole was prepared from the hydrazide by the known dehydrating cyclization reaction in $POCl_3$ as the dehydrating reagent. The bromination of this oxadiazole was not accomplished at ambient temperature, so we elevated the temperature to 70 °C and used neat CF_3COOH as the solvent. After silica gel chromatography, the pure product 2-(5-bromo-2-thienyl)-5-(perfluorobutyl)-1,3,4-oxadiazole (**2**) was isolated as a yellow solid in 90% yield.

The Marks group synthesized the n-OSC **DFHCO-4T** (Figure 1) through the Pd-mediated cross-coupling reaction of 2-perfluorohexylcarbonyl-5-bromothiophene (**3**; Figure 1) and 2,5-bis(tributylstannyl)bithiophene.[25] On the basis of this research, we expected the electron-deficient oxadiazole ring to function somewhat like a conjugated carbonyl functional group. Compound **4** was obtained by the reaction of 5,5′-bis(trimethylstannyl)-2,2′-bithiophene with 2.4 equiv of bromooxadiazole **2** by Stille coupling in the presence of a catalytic amount of $Pd(PPh_3)_4$ in a toluene/DMF mixed solvent (Scheme 2). After the usual workup, this insoluble organic semiconductor was sublimed under vacuum and acquired as a bright-red material suitable for device fabrication.

In general, oligothiophenes are too electron-rich to function as n-type OSCs themselves. After finding that the oxadiazole-ring groups were not sufficient to invert the polarity of the oligothiophenes, we introduced the fluorenone and diphenylfumaronitrile segments. The new electron-deficient diboronic

(24) Fisyuk, A. S.; Demadrille, R.; Querner, C.; Zagorska, M.; Beluse, J.; Pron, A. *New J. Chem.* **2005**, *29*, 707.

(25) (a) Yoon, M.-H.; DiBenedetto, S. A.; Russell, M. T.; Facchetti, A.; Marks, T. J. *Chem. Mater.* **2007**, *19*, 4864. (b) Yoon, M.-H.; DiBenedetto, S. A.; Facchetti, A.; Marks, T. J. *J. Am. Chem. Soc.* **2005**, *127*, 1348.

Scheme 3. Synthesis of New n-OSCs **7**−**12**[a]

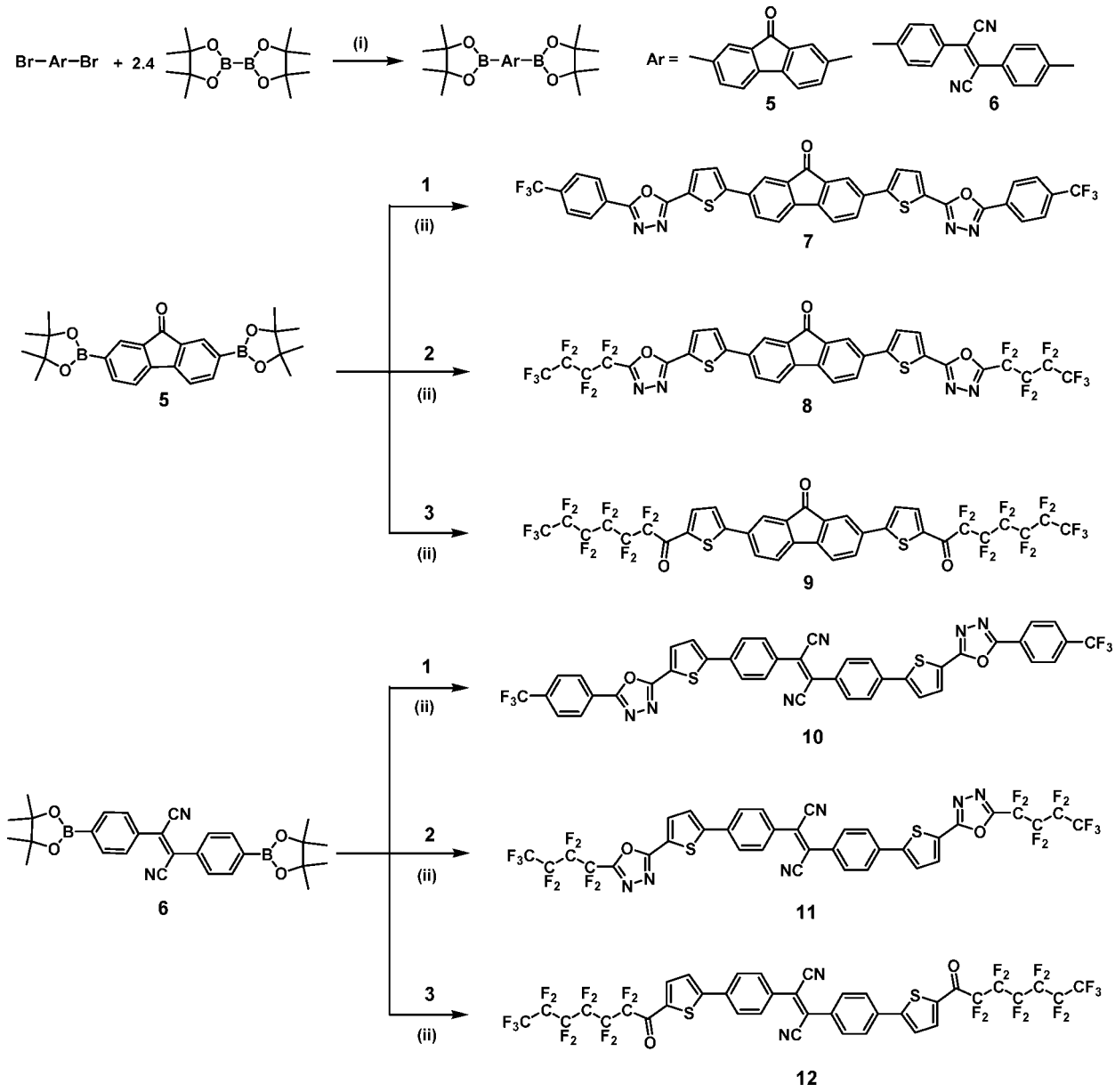

[a] (i) 5 mol % $PdCl_2$(dppf), 5 equiv KOAc, 1,4-dioxane, 100 °C. (ii) 10 mol % $Pd(PPh_3)_4$, 10 equiv Na_2CO_3 (aq), toluene, 90 °C.

esters **5** and **6** were obtained by the $PdCl_2$(dppf)-catalyzed reaction of the corresponding dibromo starting materials, bis(pinacolato)diboron, and KOAc in degassed 1,4-dioxane. After chromatography on silica gel using an EtOAc/hexane mixed eluent, the pure product **5** was isolated in 80% yield as a yellow solid, and **6** was obtained in 83% yield. Compounds **7**−**12** were synthesized from combinations of a borolane (**5** or **6**) with a bromooxadiazole (**1** or **2**) or bromothiophene (**3**) by Suzuki coupling in the presence of 10 mol % $Pd(PPh_3)_4$ as a catalyst, K_2CO_3 as a base, and 1−2 drops of Aliquat 336 as a phase-transfer agent (Scheme 3). All of these highly insoluble products were simply isolated by filtration and washing with reaction solvent in yields of 72−86%. After sublimation performed two times, the pure fluorenone compounds **7**−**9** were collected as red solids and the fumaronitrile compounds **10**−**12** as yellow solids.

Scheme 4 shows the introduction of the 1,3,4-oxadiazole ring into the centers of oligomers for comparison with compounds containing the oxadiazole at the end positions. We chose 2,5-bis(5-bromo-2-thienyl)-1,3,4-oxadiazole and 2,5-bis(4-bromophenyl)-1,3,4-oxadiazole as core parts and **3** as the end moiety with the goal of creating n-channel transistor activity. We tried to synthesize oxadiazole-containing diboronic esters **13** and **15** in a manner similar to that used for **5** and **6**. The 2,5-bis[4-(4,4,5,5-tetramethyl-1,3,2-dioxaborolanyl)-phenyl]-1,3,4-oxadiazole (**15**) was successfully prepared as a yellow solid in 84% yield using the same procedure as described for **5**. However, in the case of 2,5-bis[5-(4,4,5,5-tetramethyl-1,3,2-dioxaborolanyl)-2-thienyl]-1,3,4-oxadiazole (**13**), we failed to get the product and acquired only some insoluble oligomer as a yellow solid, even using different reaction conditions and solvents such as DMF and dimethylsulfoxide (DMSO). The

(26) Silcoff, E. R.; Asadi, A. S. I.; Sheradsky, T. *J. Polym. Sci., Part A: Polym. Chem.* **2001**, *39*, 872.

Scheme 4. Synthesis of Oxadiazole-Core Oligomers

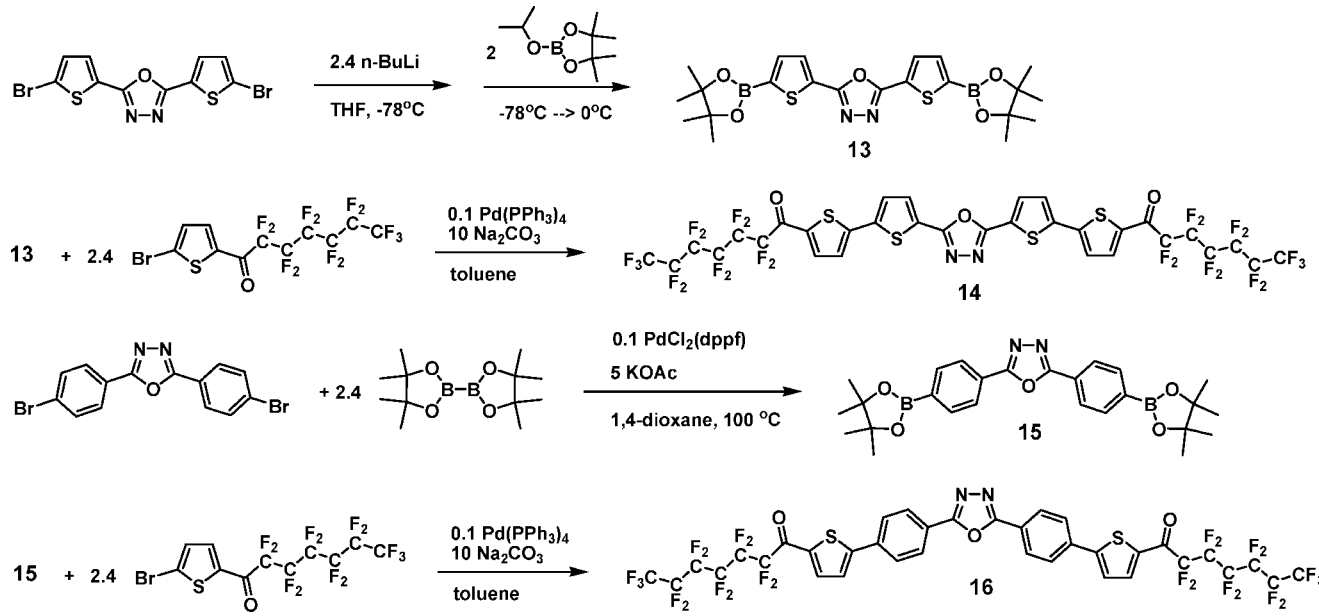

bromothiophene group, being more reactive than the bromophenyl group, may undergo a palladium-catalyzed self-coupling reaction.

We therefore tried an alternate route based on lithiation. Although organolithium reagents have a tendency to reduce oxadiazole rings, there was a notable example of a successful lithiation of 2,5-bis(2-thienyl)-1,3,4-oxadiazole with *n*-butyllithium to form a polymer with 1,2-bis(chlorodimethylsilyl)ethane.[26] Therefore, 2,5-bis(5-bromo-2-thienyl)-1,3,4-oxadiazole in freshly distilled THF was added to a solution of *n*-BuLi at −78 °C and stirred for 30 min at that temperature. After a yellow precipitate was formed, 2-isopropoxy-4,4,5,5-tetramethyl-1,3,2-dioxaborolane was added to the slurry, again at −78 °C. After silica gel column chromatography (with 1:3 ethyl acetate/hexane as eluent), **13** was isolated in relatively low yield (22%) as a yellow solid. The two novel compounds **14** and **16** were synthesized from the corresponding borolanes **13** and **15** by Suzuki coupling reaction with **3** using the same method as described above. After the usual workup, **14** and **16** were obtained as bright-yellow solids in 73 and 79% yield, respectively. Purification was accomplished by vacuum sublimation performed twice. All of these new insoluble compounds were fully characterized with MALDI-TOF mass spectrometry and elemental analysis.

X-ray Crystal Structure of 10. A single crystal of bis{4-[5-(4-trifluoromethylphenyl)-1,3,4-oxadiazol-2-yl]thiophen-2-yl}phenylfumaronitrile (**10**) was acquired during the sublimation as an orange-red prism. We also tried to obtain single crystals of **4**, **9**, and **16** through physical vapor sublimation,[27] but the crystals that formed were of insufficient quality. The molecular structure of **10** was unambiguously established by single-crystal X-ray analysis and is shown in Figure 2. Compound **10** crystallizes in a triclinic crystal system with a $P\bar{1}$ space group. All of the other crystallographic data and processing parameters are summarized in Table S1 in the Supporting Information. Two 4-[5-(4-trifluoromethylphenyl)-1,3,4-oxadiazol-2-yl]thiophen-2-yl}phenyl groups of symmetry-equivalent molecules are oriented opposite each other across the crystallographic inversion center. The bond length of the central C═C double bond is 1.330(7) Å, which is similar to the 1.338 Å bond length of the central C═C double bond of unsubstituted *trans*-stilbene.[28a] This bond length is also comparable to those in other fumaronitrile derivatives having the trans configuration: 1.341(5) Å in bis(4-bromophenyl)fumaronitrile and 1.344(7) Å in bis(3-trifluoromethylphenyl)fumaronitrile.[28b] The side view of the crystal structure (Figure 2b) reveals that this molecule does not have a flat conformation. The dihedral angle between the plane of the phenyl ring and the central NC−C═C−CN unit is ∼41°. Such nonplanarity is due to the steric hindrance between the ortho hydrogen of the benzene ring and the adjacent CN group, as in the above-mentioned compounds. This may explain why the related compound bis{5-(5-perfluorohexylcarbonylthiophen-2-yl)phenylfumaronitrile (**12**) does not have high mobility in a transistor. The stacking structure of **10** along the *b* axis of the unit cell is clearly seen (Figure 2c). The shortest distance between neighboring molecules (measured between core phenyl ring centroids) is 4.47 Å, with a dihedral angle of 41.07°. Many perpendicular $\pi-\pi$ distances are measured as 2.6−4.3 Å.

UV−Vis Spectroscopy and Thermal Properties. UV−vis spectra of the OSCs were measured in dichloromethane solution after sonication and are summarized in Table 1. The absorbance maxima of all of the derivatives are in the range 334−438 nm. The representative absorption spectra of **4**, **9**, **10**, **11**, and **14** in dichloromethane are shown in Figure S1 in the Supporting Information. The λ_{max} values are 438 nm for compound **4**, 390 nm for **9**, 334 and 413 nm for **10**, 334 and 390 nm for **11**, and 405 nm for **14**. It was possible to determine the optical-energy band gaps (E_g) from the absorbance onset of the UV−vis spectra. These values were between 2.34 and 2.56 eV. Compound **12** showed the largest band gap because of the strongly electron-withdrawing dicyano core and perfluorocarbonyl end group, which reduce the overall polarization within the molecule.

The melting points of the OSCs were exactly measured by differential scanning calorimetry (DSC) and are given in the Experimental Section. All of the compounds showed a reversible phase change during the heating and cooling. Figure S3 in the

(27) Laudise, R. A.; Kloc, C.; Simpkins, P. G.; Siegrist, T. *J. Cryst. Growth* **1998**, *187*, 449.

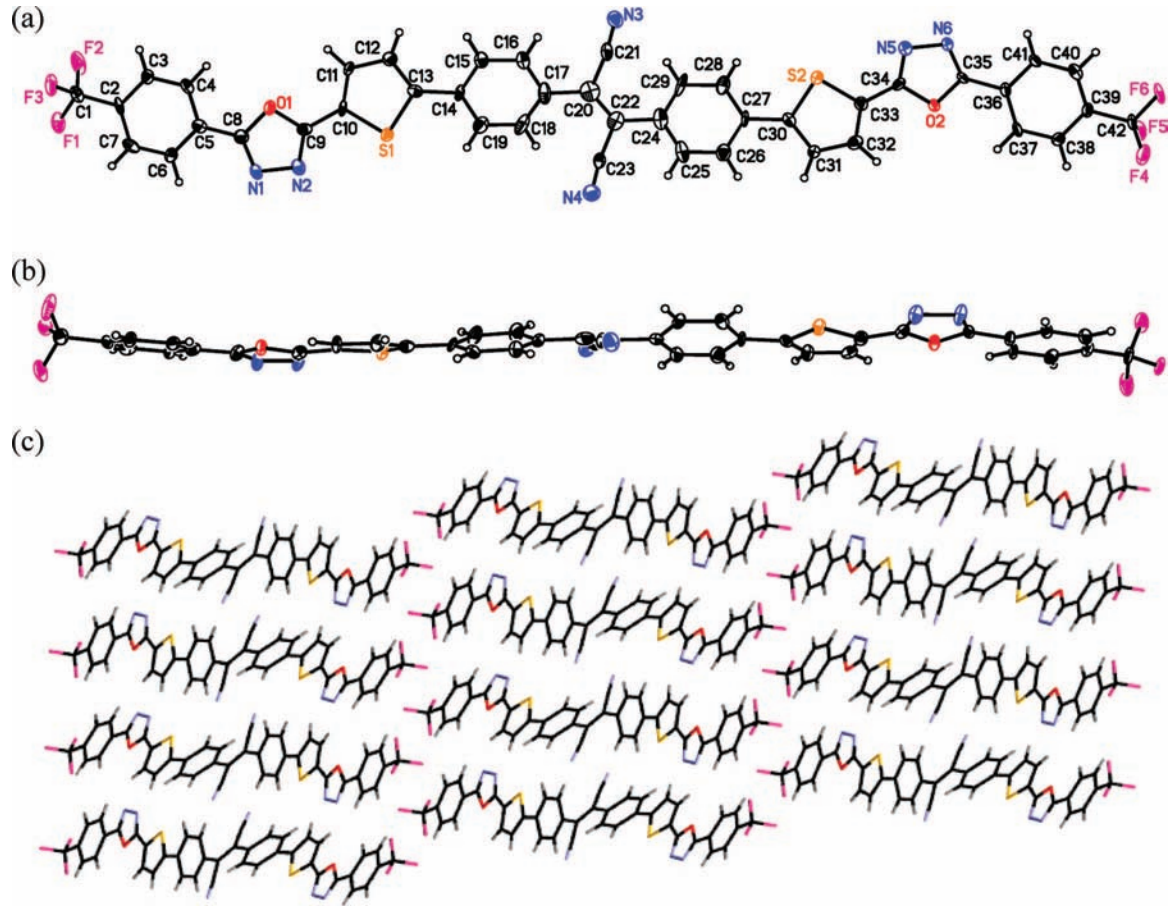

Figure 2. X-ray crystal structure of **10** with 50% probability thermal ellipsoids depicted: (a) top view; (b) side view. (c) Packing diagram for **10**.

Table 1. Spectroscopic, Electrochemical, and Theoretical Data for Oxadiazole-Based Oligomers and New n-Type OSCs

			experimental			theoretical		
compound	λ_{max} (nm)[a]	E^{red}_{onset} (V)[b]	E_{HOMO} (eV)	E_{LUMO} (eV)	E_g (eV)[c]	E_{HOMO} (eV)	E_{LUMO} (eV)	E_g (eV)[d]
4	438	−1.09	−5.99	−3.56	2.43	−5.63	−2.86	2.77
7	410	−0.82	−6.22	−3.83	2.39	−5.82	−2.86	2.96
8	418	−0.78	−6.21	−3.87	2.34	−6.09	−2.99	3.10
9	390	−0.77	−6.30	−3.88	2.42	−6.31	−3.21	3.10
10	334, 413	−0.86	−6.20	−3.79	2.41	−6.04	−3.18	2.86
11	344, 390	−0.77	−6.42	−3.88	2.54	−6.34	−3.32	3.02
12	381, 423	−0.69	−6.52	−3.96	2.56	−6.58	−3.46	3.13
14	405	−0.93	−6.23	−3.72	2.51	−6.09	−3.21	2.88
16	397	−0.99	−6.07	−3.66	2.41	−6.34	−3.02	3.32

[a] Measured in dichloromethane solution. [b] Measured in a 0.1 M solution of Bu_4NPF_6 in dichloromethane with a Pt electrode and a Ag/AgCl reference electrode (0.045 V vs SCE). The electron affinity (EA) is given by EA = E^{red}_{onset} + 4.7 V. [c] Calculated from the optical absorption onset. [d] HOMO/LUMO energy gap of the B3LYP/6-31G(d)-optimized structure in the gas phase.

Supporting Information shows selected DSC thermograms for **4** and **9**. The thermogram of **4** shows the major endothermic melting peak at 288 °C and its corresponding exothermic crystallization peak at 283 °C. Compound **9** undergoes two thermal transitions. When the sample is heated, the first and second endothermic peaks are exhibited at 122 and 290 °C. When it is cooled, the corresponding exothermic peaks are shown sharply at 108 and 287 °C, respectively. All of the OSCs are thermally stable with respect to thermal deposition in vacuum.

Electrochemistry and DFT Calculations. The electrochemical analysis is important for understanding the highest occupied molecular orbital (HOMO) and lowest unoccupied molecular orbital (LUMO) energy levels, charge injection, the charge-carrier type, and substituent effects. All of the electrochemical measurements were carried out in dichloromethane solution under N_2 except for compound **4**, which was measured in THF solution because of its low solubility; each solution contained 1 mM oligomer and 0.1 M tetrabutylammonium hexafluorophosphate (NBu_4PF_6), and the scan rate was 100 mV/s. A platinum disk and platinum wire were used as the working and counter electrodes, respectively. We used Ag/AgCl in 3 M NaCl aqueous solution as a reference electrode. Figure 3 and Figure S2 in the Supporting Information show representative cyclic voltammetry (CV) curves for **10** and for **9**, **12**, and **16**, respectively, with full cycles. All of the derivatives showed the reduction potentials clearly, and most of them have one or two reversible (**10** and **16**), quasireversible (**4**, **7**, and **12**), or irreversible (**8**, **9**, **11**, and **14**) reduction waves ranging between −0.72 and −1.50 V versus Ag/AgCl. Because the oxidation

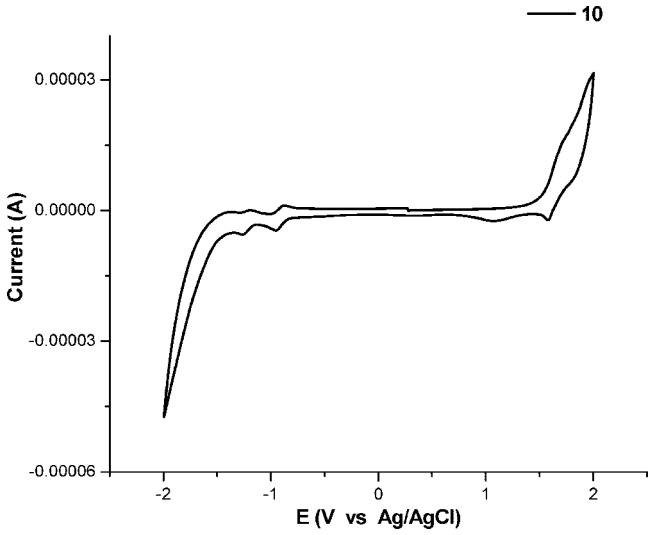

Figure 3. Cyclic voltammogram of **10**.

waves were similar to solvent peaks, it was difficult to define oxidation potentials except for the fumaronitrile series (**10**−**12**), which show quasireversible or irreversible oxidation waves. The reduction onset potential values (E^{red}_{onset}) obtained versus Ag/AgCl are listed in Table 1. From these potentials, the LUMO levels were determined. To estimate the HOMO and LUMO energy levels, we converted the acquired values of E^{red}_{onset} to values versus the SCE (saturated calomel electrode) reference standard by subtracting 0.045 V from the original reduction onset.[29] Assuming that the energy level of SCE is 4.7 eV below the vacuum level, we determined the LUMO energy levels (in eV) using the equation $E_{LUMO} = -(E^{red}_{onset} + 4.7)$.[30] The HOMO energy levels were obtained by subtracting the E_g values (calculated from the optical absorption onsets of the UV−vis spectra) from the LUMO levels; they are summarized in Table 1. Interestingly, compound **10** showed two reversible reduction (n-doping) processes and one quasireversible oxidation (p-doping) process. Electrochemical reduction (n-doping) of **10** starts at about −0.86 V (vs Ag/Ag^+) and gives two peaks at −0.95 and −1.26 V. The corresponding n-dedoping peaks appear at −0.87 and −1.19 V, respectively. On the basis of the oxidation onset potential E^{ox}_{onset} (1.50 V vs Ag/AgCl), we could obtain the estimated electrochemical HOMO energy level as −6.15 eV using the equation $E_{HOMO} = -(E^{ox}_{onset} + 4.7)$. This result agrees well with the value of −6.20 eV calculated from the electrochemical LUMO energy level and the optical-energy band gap. To realize air-stable n-channel OFETs, highly reduced LUMO levels (below −4.0 eV) are required to prevent oxidation by oxygen.[31] On the basis of this approach, organic semiconductor **12** looks somewhat promising as an n-OSC among the set of materials.

Because of the difficulty in producing high-quality single crystals, density functional theory (DFT) calculations were employed to understand the electronic structures (the electronic distributions of the HOMO and LUMO frontier orbitals and the energy band gap) and molecular geometries. Figure 4 shows the HOMO and LUMO frontier orbitals of the B3LYP/6-31G(d)-optimized spatial structures. While most of the HOMOs exhibit similar patterns of spatial characteristics, the LUMO

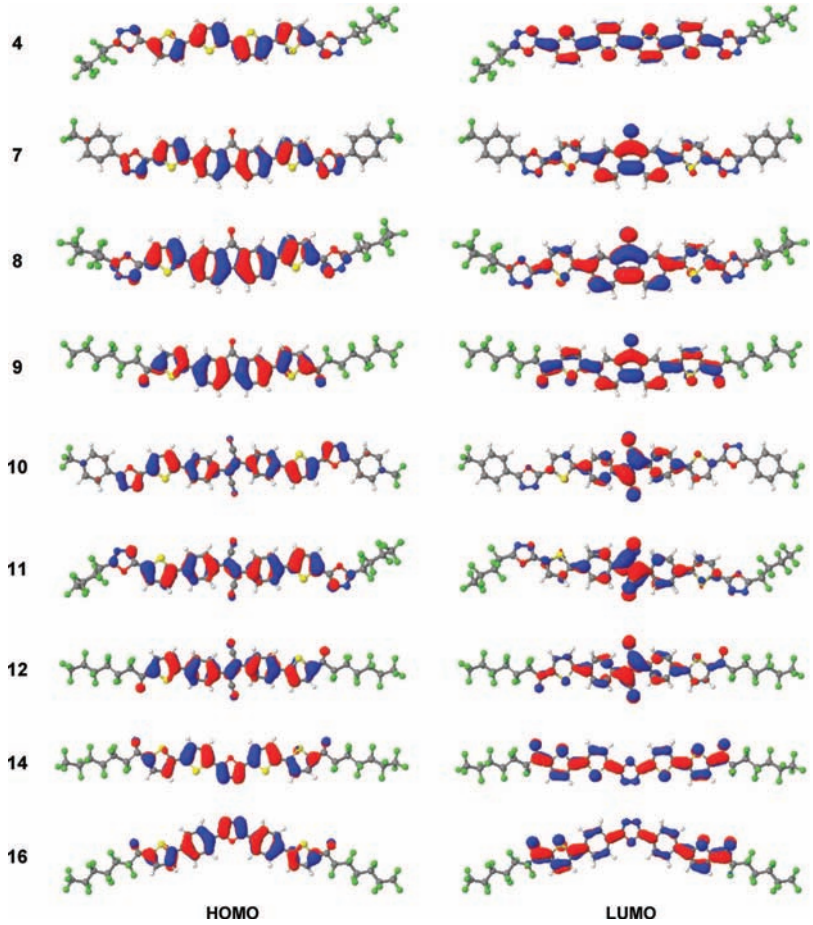

Figure 4. (left) HOMOs and (right) LUMOs of **4**, **7**−**12**, **14**, and **16**. The figures were generated using Jmol software.

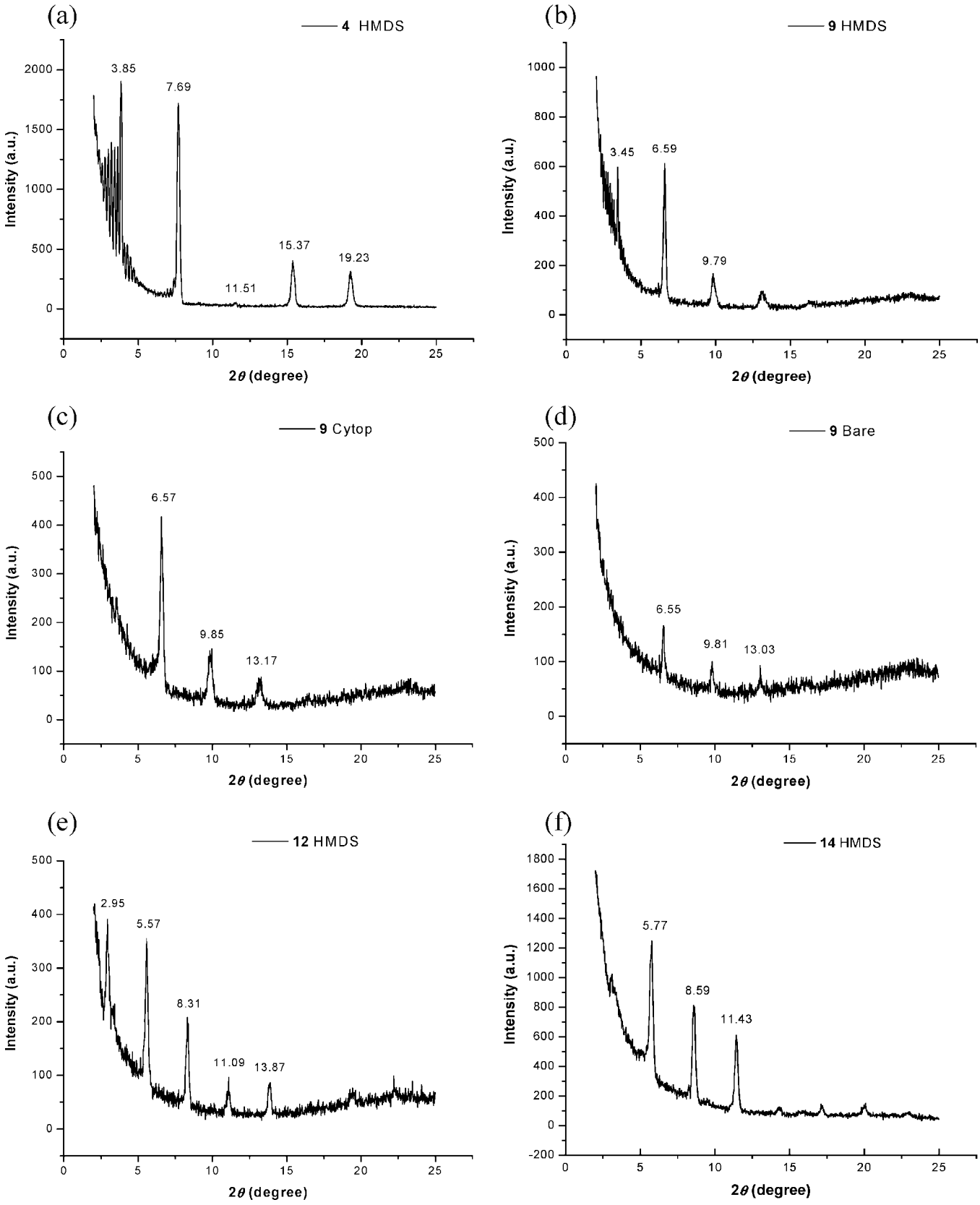

Figure 5. XRD scans of films of (a) **4** on HMDS; **9** on (b) HMDS, (c) Cytop, and (d) bare SiO_2; (e) **12** on HMDS; and (f) **14** on HMDS-treated SiO_2 at 120 °C deposition.

topologies vary. The poor conjugation between the central portion and the terminal carbonyl fragments in the HOMOs of **9**, **12**, **14**, and **16** is consistent with the proposal by Yoon et al.[25a] that the carbonyl (CO) nonbonding orbital and the filled π orbitals of the core cannot interact well for symmetry reasons. Interestingly, the oxadiazole ring placed at the side region is

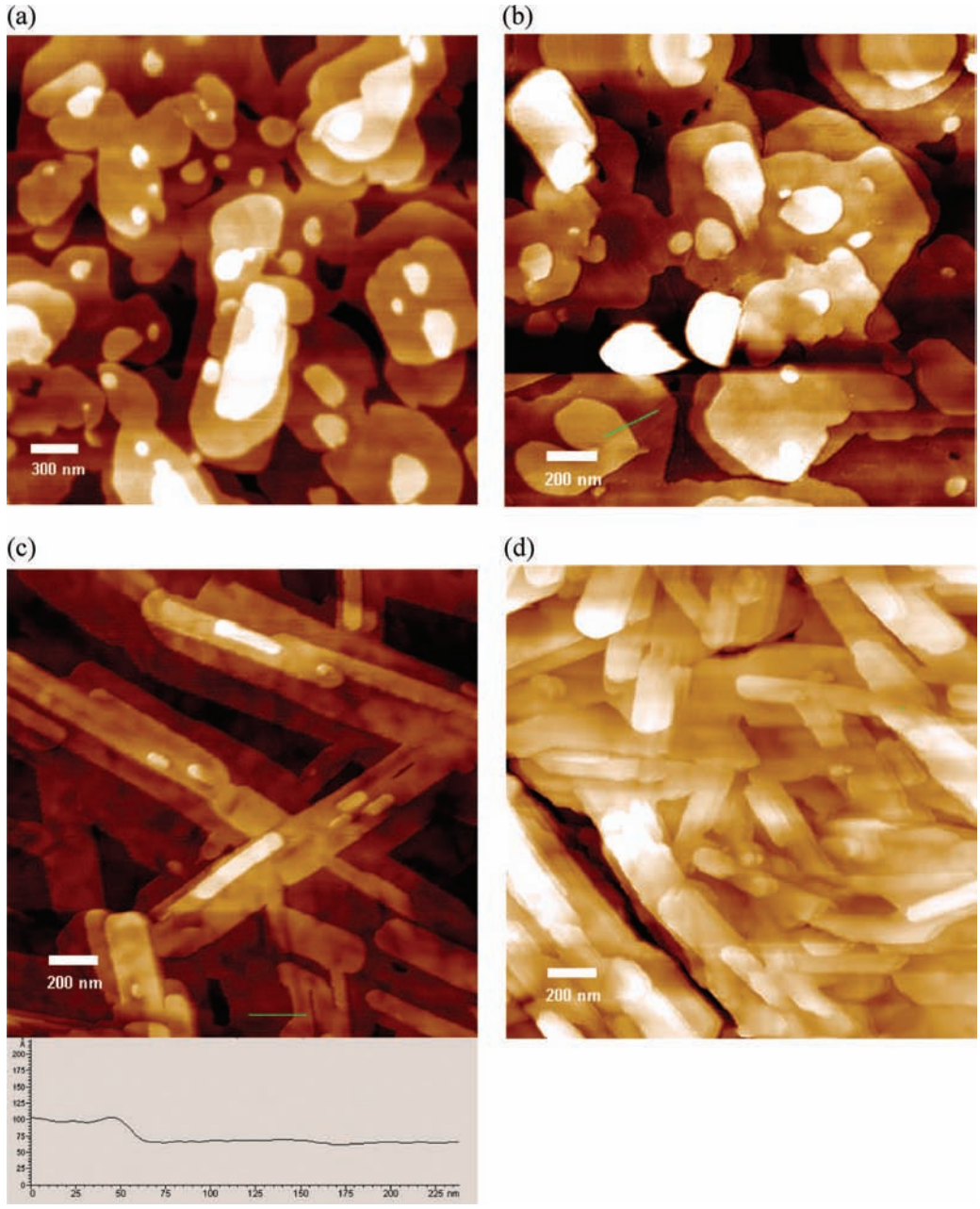

Figure 6. AFM topography of thin films of (a) **4**, (b) **9**, and (c) **12** on HMDS and (d) **12** on Cytop.

relatively weakly conjugated, perhaps even breaking the conjugation with the terminal trifluoromethylphenyl group. On the other hand, the LUMOs in this series are fully extended to the carbonyl groups. Although the 1,3,4-oxadiazole is widely assumed to be electron-withdrawing, the DFT calculations reveal that the electron densities of the oxadiazole in the LUMO are negligible compared with those in the thiophene or phenyl rings. These results are matched well with previous reports.[32] The electronic structures of the LUMOs of **14** and **16** reveal that the electron-accepting power of oxadiazole placed at the center is less than that of the terminal carbonyl, so the oxadiazole has little benefit in facilitating the injection of electrons from the electrode. These calculated LUMO energies are generally in good agreement with the experimental trends in the reduction potentials (Table 1). For example, the theoretical LUMO energy values of the fumaronitrile derivatives decreased in going from **10** (−3.18 eV) to **12** (−3.46 eV), which is quite consistent with the trend in the experimental values: −3.79 eV (**10**) → −3.88 eV (**11**) → −3.96 eV (**12**). Similar trends were also observed in the E_{HOMO} and E_g values in the same series. In summary, the order of electron-withdrawing abilities based on the LUMO levels is fumaronitrile > fluorenone > oxadiazole.

Solid-State Thin Film Properties. X-ray diffraction (XRD) and atomic force microscopy (AFM) were performed to investigate the morphologies and crystallinities of films of the semiconductors. These were characterized as 50 nm thin films thermally vacuum-deposited on variously surface-treated Si/SiO_2. Table S2 in the Supporting Information summarizes the *d*-spacings (*d*) extracted from Bragg progression reflections in conventional $\theta-2\theta$ scans and the computed molecular long-axis lengths (*l*) and tilt angles (φ). The XRD scans show that most of the films are highly crystalline at substrate temperatures of 90 and 120 °C. Representative XRD scans of **4**, **9**, **12**, and **14** are shown in Figure 5. In the case of **4**, there are two

Table 2. OFET Performance Measured under Air for **4** and Vacuum[a] for **9**, **11**, and **12**

compound	type	T_s (°C)	surface treatment	μ ($cm^2\ V^{-1}\ s^{-1}$)	μ_{max} ($cm^2\ V^{-1}\ s^{-1}$)	I_{on}/I_{off}	V_{th} (V)
4	p	60	bare	0.015	0.016	1×10^5	−75
			HMDS	0.051	0.057	2×10^5	−38
		90	bare	0.016	0.018	3×10^5	−58
			HMDS	0.064	0.065	5×10^5	−35
		120	bare	0.013	0.016	3×10^6	−45
			HMDS	0.106	0.114	4×10^5	−25
			ODTS	**0.137**	**0.181**	$\mathbf{5 \times 10^5}$	**−24**
			Cytop[b]	0.047	0.055	4×10^4	−40
9	n	120	bare	0.0005	0.0008	6×10^3	76
			HMDS	0.003	0.0034	1×10^4	60
			Cytop[b]	**0.01−0.06**	**0.063**	$\mathbf{1 \times 10^5}$	**57**
		130	HMDS	0.006	0.007	1×10^4	68
11	n	120	bare	0.0001	0.0003	5×10^3	83
			HMDS	0.001	0.0012	3×10^4	73
			Cytop[b]	0.0016	0.002	1×10^4	90
12	n	120	bare	0.0007	0.001	3×10^3	71
			HMDS	0.024	0.027	3×10^6	50
			Cytop[b]	0.019	0.025	2×10^5	64

[a] Measured at a vacuum-probe station under a pressure of 10^{-3} Torr. [b] A 9% Cytop solution (CTL-809M, Asahi Glass company) was spin-coated on the Si/SiO_2 (300 nm) substrate (2000 rpm for 60 s) and then cured for 1 h at 120 °C.

dominant peaks and three weak peaks from third to fifth order on a hexamethyldisilazane (HMDS) surface (Figure 5a). The molecular long-axis tilt angle with respect to the surface normal, defined from the *d*-spacing and the computed molecular length, is 38.2°. Interestingly, there is a series of small peaks on the shoulder of the first-order peak. These oscillations have been attributed by See et al.[14d] to two possible phenomena: (i) Kiessig fringes and (ii) Laue oscillations. Kiessig fringes indicate excellent ordering at the semiconductor/insulator interface as well as the surface of the film. Laue oscillations mean excellent crystallinity throughout the thickness of the film. In other words, the appearance of either type of oscillation indicates that the thin films are well-ordered and highly crystalline. Compound **9** has a long-axis tilt angle of 35° regardless of surface. The intensities of the peaks on HMDS and Cytop are similar, but the thin film of **9** on the bare SiO_2 surface shows decreased crystallinity (Figure 5b−d). Compound **12** shows five clear peaks and exhibits a slightly lower inclination in its molecular orientation, with estimated long-axis tilt angles of 26.2° on HMDS (Figure 5e) and 27.5° on Cytop. Compound **14**, with the oxadiazole placed in the center, is well-ordered and has high crystallinity on the basis of XRD. However, there is no transistor behavior with this molecule. Therefore, a chemical or electronic effect must limit the charge-carrier mobility.

Figure 6a−c shows representative AFM topography images of evaporated thin films of **4**, **9**, and **12** on an HMDS-treated Si/SiO_2 substrate at $T_{sub} = 120$ °C. The AFM images of **4** and **9** indicate that these films have similar morphologies. The thin film of **4** consists of grains with sizes of 0.4−0.6 μm and has a surface roughness (Ra) of 2.25 nm. The grain sizes of **9** are estimated to be 0.4−0.8 μm, and the measured Ra is 3.54 nm. On the other hand, in the case of the film of **12**, fiberlike structures are formed on both HMDS-treated and Cytop spin-coated substrates. As shown in Figure 6c,d, the rod-type grains on the HMDS-treated substrate are better ordered than those on Cytop substrate. In addition, the grains on the HMDS-treated substrate are somewhat larger and smoother (rod width, ∼0.1 μm; rod length, ∼2.0 μm; Ra = 3.64 nm) than the grains on Cytop (rod width, ∼0.1 μm; rod length, ∼1.0 μm; Ra = 4.79 nm). These results are plausible reasons to explain why the FET performance of **12** is slightly better on HMDS than on Cytop. The height profile of **12** reveals the smallest terrace step size of ∼3.0 nm, consistent with the size of the long axis of the oligomer, 3.18 nm, estimated by XRD analysis (Table S2 in the Supporting Information).

Field-Effect Transistors. Top-contact configurations of thin film transistors of semiconductors were fabricated, and the details are described in the Experimental Section. All of the films were vacuum-deposited in a thermal evaporator on bare and HMDS-treated n^{++}-Si/SiO_2 substrates with various deposition temperatures (T_s). The fabrication was completed by evaporating gold through a shadow mask to form source and drain electrodes. Devices made at a substrate temperature of 120 °C showed the highest mobility, so under that condition we tried the deposition on various substrate treatments or dielectrics, including octadecyltrimethoxysilane (ODTS)-treated Si/SiO_2 substrates and spin-coated Cytop dielectric layers on Si/SiO_2. In the case of oxadiazole n-type OSCs, Al was also tried as the source/drain contact material. The measurements were performed under air unless otherwise noted. When n-channel OFETs were characterized under vacuum at a temperature of 25 °C, at least 3−5 channels were tested in different regions of a film, and the average is reported. The mobilities were calculated from the saturation regime and fitted in the regions of largest slope.[33] Average mobility (μ), maximum mobility (μ_{max}), current on/off ratio (I_{on}/I_{off}), and threshold voltage (V_{th}) data for OFETs based on semiconductors **4**, **9**, **11**, and **12** are summarized in Table 2.

Although the OSC **4** has an electron-withdrawing oxadiazole end group with a perfluorobutyl chain directly attached, the

(28) (a) Hoekstra, A.; Meertens, P.; Vos, A. *Acta Crystallogr., Sect. B* **1975**, *31*, 2813. (b) Yeh, H.-C.; Wu, W.-C.; Wen, Y.-S.; Dai, D.-C.; Wang, J.-K.; Chen, C.-T. *J. Org. Chem.* **2004**, *69*, 6455.
(29) Tsujimura, S.; Kawaharada, M.; Nakagawa, T.; Kano, K.; Ikeda, T. *Electrochem. Commun.* **2003**, *5*, 138.
(30) (a) Thompson, B. C.; Kim, Y.-G.; Reynolds, J. R. *Macromolecules* **2005**, *38*, 5359. (b) Bard, A. J.; Faulkner, L. R. *Electrochemical Methods: Fundamentals and Applications*, 2nd ed.; Wiley: New York, 2001. (c) Scudiero, L.; Barlow, D. E.; Mazur, U.; Hipps, K. W. *J. Am. Chem. Soc.* **2001**, *123*, 4073. (d) Richardson, D. E. *Inorg. Chem.* **1990**, *29*, 3213.
(31) Jones, B. A.; Facchetti, A.; Wasielewski, M. R.; Marks, T. J. *J. Am. Chem. Soc.* **2007**, *129*, 15259.
(32) (a) Jansson, E.; Jha, P. C.; Ågren, H. *Chem. Phys.* **2006**, *330*, 166. (b) Risko, C.; Zojer, E.; Brocorens, P.; Marder, S. R.; Brédas, J.-L. *Chem. Phys.* **2005**, *313*, 151.
(33) Horowitz, G.; Hajlaoui, M. E.; Hajlaoui, R. *J. Appl. Phys.* **2000**, *87*, 4456.

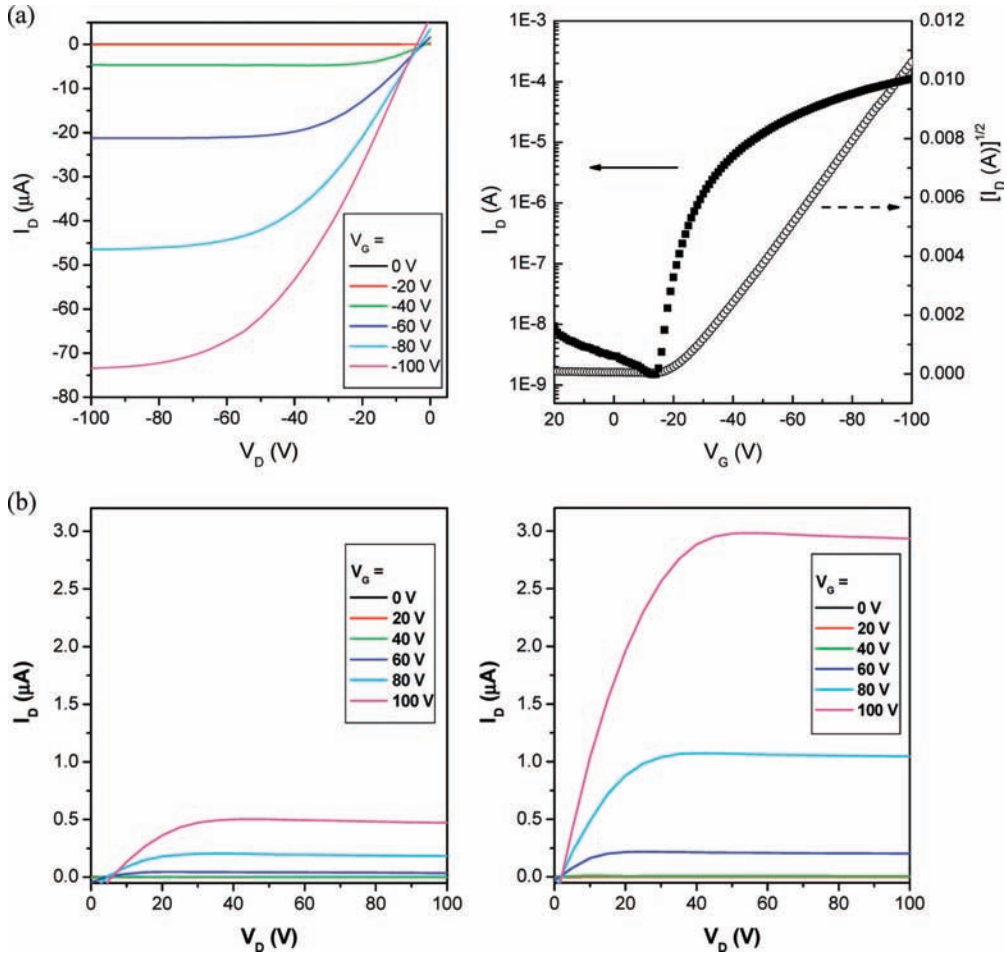

Figure 7. (a) p-Channel OFET behavior of **4** on HMDS-treated SiO_2 with Au electrodes fabricated at a substrate temperature of 120 °C. (b) n-Channel OFET behavior of **9** on (left) HMDS-treated and (right) Cytop-treated SiO_2 with Au electrodes fabricated at a substrate temperature of 120 °C.

transistor of **4** showed only p-channel behavior both in air and vacuum. Figure 7a shows characteristics of the best-performing transistor type, having Au as the source and drain electrodes on an HMDS-treated Si/SiO_2 dielectric. At $T_s = 120$ °C, the hole mobilities exceeded 0.1 $cm^2\ V^{-1}\ s^{-1}$ on both HMDS- and ODTS-treated devices. The mobilities of devices with **4** on bare Si/SiO_2 varied little with substrate temperature, but the threshold voltage slightly decreased as the temperature increased. In the case of HMDS-treated devices, deposition at 120 °C showed a hole mobility of 0.11 $cm^2\ V^{-1}\ s^{-1}$, a threshold voltage of −25 V, and an I_{on}/I_{off} ratio of 4×10^5. Under the same conditions, ODTS-treated devices gave the highest average value of mobility, 0.14 $cm^2\ V^{-1}\ s^{-1}$ (with a maximum value of 0.18 $cm^2\ V^{-1}\ s^{-1}$), a threshold voltage of −24 V, and an I_{on}/I_{off} ratio of 5×10^5. The reason why **4** shows p-channel behavior is not obvious, but apparently its combination of HOMO and LUMO energies (−5.99 and −3.56 eV, respectively, based on CV and −5.63 and −2.86 eV, respectively, based on DFT calculations) facilitates hole-only thin film carrier transport. Because of insufficient LUMO energy of OSC **4,** the semiconductor has a small electron affinity and does not support n-channel transistor operation when contacted with a gold electrode, which has a work function of ∼5 eV.

There is no significant degradation in the performance of the transistors over a period of 3 months in the ambient environment. This good air stability of the p-channel transistors based on OSC **4** is a benefit of the large ionization potential (almost 6 eV). Similar long-term air stability was reported by Meng, Klauk, and co-workers.[34]

In spite of many attempts, oxadiazole-based OSCs (including **14** and **16**) showed no transistor behavior under air or vacuum, except for **11**. Even though we tested the low work-function Al electrode (4.3 eV) instead of Au (5.1 eV) to facilitate electron injection from the electrode to the organic semiconductor, only **11** revealed n-channel OFET behavior, under a vacuum of 10^{-3} torr. This phenomenon is due to the strong electron-accepting ability of the fumaronitrile core. To the best of our knowledge, compound **11** is the first example of an oxadiazole-containing n-OSC used in an OFET. However, the transistor properties did not compare favorably with those of other reported n-type organic transistors.[35] The electron mobility was 0.001 $cm^2\ V^{-1}\ s^{-1}$, the threshold voltage 73 V, and the I_{on}/I_{off} ratio 3×10^4 on the HMDS-treated Si wafer using 120 °C substrate treatment during deposition. Under the same conditions, the mobility was 0.0016 $cm^2\ V^{-1}\ s^{-1}$, the threshold voltage 90 V, and the I_{on}/I_{off} ratio 1×10^4 on Cytop spin-coated Si/SiO_2. The poor transistor

(34) (a) Meng, H.; Sun, F.; Goldfinger, M. B.; Gao, F.; Londono, D. J.; Marshal, W. J.; Blackman, G. S.; Dobbs, K. D.; Keys, D. E. *J. Am. Chem. Soc.* **2006**, *128*, 9304. (b) Klauk, H.; Zschieschang, U.; Weitz, R. T.; Meng, H.; Sun, F.; Nunes, G.; Keys, D. E.; Fincher, C. R.; Xiang, Z. *Adv. Mater.* **2007**, *19*, 3882.

(35) (a) Mamada, M.; Nishida, J.-i.; Kumaki, D.; Tokito, S.; Yamashita, Y. *Chem. Mater.* **2007**, *19*, 5404. (b) Ando, S.; Murakami, R.; Nishida, J.-i.; Tada, H.; Inoue, Y.; Tokito, S.; Yamashita, Y. *J. Am. Chem. Soc.* **2005**, *127*, 14996.

behavior is related to the relatively weak crystallinity of the film of **11** (Figure S4 in the Supporting Information).

Two other OSCs, **9** and **12**, which contain no oxadiazole rings, showed n-channel transistor behavior in vacuum, and the highest mobility was obtained at 120 °C deposition. Compound **9** showed inconsistent mobility on the order of 0.01 $cm^2\ V^{-1}\ s^{-1}$, in one case reaching a mobility of 0.06 $cm^2\ V^{-1}\ s^{-1}$ (on Cytop spin-coated SiO_2) but having a more consistent mobility of 0.003 $cm^2\ V^{-1}\ s^{-1}$ on HMDS-treated SiO_2. I_D-V_D curves are shown in Figure 7b. We obtained double the electron mobility, 0.006 $cm^2\ V^{-1}\ s^{-1}$, on HMDS-treated SiO_2 at 130 °C deposition. This is in accordance with the findings of Chua et al.,[36] in which use of a hydrophobic BCB dielectric eliminated silanol traps responsible for trapping electrons at the interface. The device using **12** showed a different pattern in the value of the mobility that that using **9**: the mobility of 0.024 $cm^2\ V^{-1}\ s^{-1}$ on HMDS-treated SiO_2 was slightly higher than the value of 0.019 $cm^2\ V^{-1}\ s^{-1}$ on Cytop spin-coated SiO_2. The HMDS-treated device using **12** had the lowest value of the threshold voltage, 50 V, among this series of new n-OSCs, and the I_{on}/I_{off} ratio was 3×10^6. This inconsistency of the effect of the Cytop dielectric is not immediately explicable.

Except for devices made from **12**, none of the transistors could be operated in air. Figure S5 in the Supporting Information shows n-Channel OFET behavior of **12** on Cytop-treated SiO_2 with Au electrodes in air, but the OFET properties were poor: the mobility was 0.0001 $cm^2\ V^{-1}\ s^{-1}$ with a threshold voltage of 90 V and an I_{on}/I_{off} ratio of 2×10^4 on HMDS-treated SiO_2 and 0.0007 $cm^2\ V^{-1}\ s^{-1}$ with a threshold voltage of 79 V and an I_{on}/I_{off} ratio of 1×10^2 on Cytop spin-coated Si/SiO_2.

Conclusions

We have synthesized a new series of heterocyclic oligomers based on the oxadiazole ring and the other electron-deficient cores fluorenone and fumaronitrile to investigate the oligomers as electron carriers. The physical properties of the materials were fully characterized by UV−vis spectroscopy, DSC, CV, and DFT calculations. Thin films were deposited at different substrate temperatures on variously coated Si/SiO_2 substrates and then studied by XRD and AFM. Although the structure of **4** was designed for n-channel activity, the thin film devices revealed p-channel behavior, with a significant average hole mobility of 0.14 $cm^2\ V^{-1}\ s^{-1}$ (maximum value 0.18 $cm^2\ V^{-1}\ s^{-1}$), a threshold voltage of −24 V, and an I_{on}/I_{off} ratio of 5×10^5 at 120 °C deposition on ODTS-treated Si/SiO_2. Compound **11** is the first example of an oxadiazole-containing OSC as an n-channel OFET, but the transistor mobilities were only moderate. When we eliminated oxadiazole from the backbone (**9** and **12**), the two resulting OSCs showed n-channel OFET behavior. The device built from **9** had electron mobility in vacuum of 0.01−0.06 $cm^2\ V^{-1}\ s^{-1}$ on Cytop spin-coated SiO_2, in contrast to the value of 0.003 $cm^2\ V^{-1}\ s^{-1}$ on HMDS-treated SiO_2. The mobility of **12** was 0.024 $cm^2\ V^{-1}\ s^{-1}$ on HMDS-treated SiO_2 in vacuum. These are the first fluorenone and fumaronitrile-based n-OSCs demonstrated in transistors. On the basis of our research, oxadiazoles are not promising subunits for air-stable n-channel transistors with high electron mobility, despite their long history of use as electron-injection layers in OLEDs. The fumaronitrile and fluorenone subunits appear to be more applicable by comparison. In particular, annelated fumaronitriles that maintain the planarity of the conjugation should be promising.

Experimental Section

General. All of the experiments were performed under a nitrogen atmosphere by standard Schlenk techniques. THF was freshly distilled from sodium benzophenone under N_2 prior to use. ^1H and ^{13}C NMR spectra were recorded on Bruker Avance (300 MHz/400 MHz) spectrometers. Mass spectrometry (MS) analyses were performed on MALDI-TOF mass spectrometer at the University of Kentucky Mass Spectrometry Facility. The absorption spectra were measured using a Varian Cary 50 UV−vis spectrometer. DSC measurements were carried out using a TA DSC Q20 modulated instrument at a heating rate of 5 °C/min and a cooling rate of 4 °C/min under a nitrogen atmosphere. Except in the case of **4**, where THF was used as the solvent, all of the electrochemical measurements were carried out in dichloromethane solutions containing 1 mM complex and 0.1 M NBu_4PF_6 as the supporting electrolyte at room temperature using an EG&G Instruments 263A potentiostat/galvanostat. The cyclic voltammograms were obtained at a scan rate of 100 mV/s. A platinum disk and platinum wire were used as the working and counter electrodes, respectively, and Ag/AgCl in 3 M NaCl aqueous solution was used as the reference electrode. 4-(Trifluoromethyl)benzoyl chloride was purchased from SynQuest Laboratories Inc., perfluoropentanoic anhydride from Matrix Scientific, 2,7-dibromo-9-fluorenone from Oakwood Products, Inc., and bis(pinacolato)diboron from AK Scientific, Inc. All of the other chemicals were purchased from Aldrich, Alfa Aesar, or TCI and used without further purification. $Pd(PPh_3)_4$,[37] 5,5′-bis(trimethylstannyl)-2,2′-bithiophene,[38] bis(4-bromophenyl)fumaronitrile,[21b] 2,5-bis(5-bromo-2-thienyl)-1,3,4-oxadiazole,[39] and 2,5-bis(4-bromophenyl)-1,3,4-oxadiazole[40] were prepared according to the literature. Numerical quantities over arrows in schemes are mole equivalents.

Device Fabrication and Characterization. Heavily n-doped silicon wafers with 300 nm thermally grown SiO_2 dielectric layers were purchased from Process Specialties. The gate dielectric capacitance was calculated to be 11.5 nF/cm^2 assuming a dielectric constant of 3.9 for SiO_2. Wafers were cleaned using piranha solution (a 3:1 mixture of sulfuric acid and 30% hydrogen peroxide; **Caution!** *piranha solution is extremely corrosive and reactive*), deionized water, acetone, and isopropyl alcohol followed by oxygen plasma. The cleaned substrates were treated with the HMDS or ODTS vapor to make the surface hydrophobic. A 9% Cytop solution (CTL-809M, Asahi Glass company) was spin-coated on the Si/SiO_2 (300 nm) substrate (2000 rpm for 90 s) and then cured for 1 h at 120 °C to make the Cytop dielectric-coated Si/SiO_2 substrate. The capacitance of the spin-coated Cytop dielectric layer was measured to be 1.8 nF/cm^2 using an Agilent 4284A LCR meter. Thin films (50 nm) of organic semiconductor were deposited by vacuum evaporation (at pressures of $<10^{-5}$ Torr) at a growth rate of 1.0−2.0 Å/s at various substrate temperatures. All of the devices were in the top-contact configuration with gold electrodes (thicknesses of ∼50 nm) thermally evaporated through a shadow mask after organic deposition. The channel widths were 6 mm and the channel lengths 250 μm. Devices were evaluated in air using an Agilent 4155C semiconductor analyzer with the ICS lite software and in vacuum using a Keithley 4200 semiconductor analyzer in an ST-500-1 vacuum triaxial probe station purchased from Janis Research Company, Inc. The mobilities were calculated from the saturation regime and fitted in the regions of highest slope.[33]

Thin Film Characterization. X-ray diffraction scans of thin films (50 nm) were acquired in the Bragg−Brentano ($\theta-2\theta$)

(36) Chua, L. L.; Zaumseil, J.; Chang, J. F.; Ou, E. C. W.; Ho, P. K. H.; Sirringhaus, H.; Friend, R. H. *Nature* **2005**, *434*, 194.

(37) Coulson, D. R. *Inorg. Synth.* **1972**, *13*, 121.

(38) Murphy, A. R.; Liu, J.; Luscombe, C.; Kavulak, D.; Fréchet, J. M. J.; Kline, R. J.; McGehee, M. D. *Chem. Mater.* **2005**, *17*, 4892.

(39) Huang, P.-H.; Shen, J.-Y.; Pu, S.-C.; Wen, Y.-S.; Lin, J. T.; Chou, P.-T.; Yeh, M.-C. P. *J. Mater. Chem.* **2006**, *16*, 850.

(40) Zhan, X.; Liu, Y.; Wu, X.; Wang, S.; Zhu, D. *Macromolecules* **2002**, *35*, 2529.

geometry with Cu Kα radiation and a monochromator using a Phillips X-pert Pro X-ray diffraction system. All $\theta-2\theta$ scans were calibrated with the reflection of the Si (100) substrates. Scans used a step size of 0.02° and a time per step of 2 s. AFM images were observed by tapping-mode AFM (Molecular Imaging PicoPlus).

Computational Methods. All of the DFT calculations were performed with the Gaussian 03 program package (Gaussian, Inc.). DFT calculations are reliable in predicting molecular geometries and energies because of the involvement of the electron correlation effect.[41] The starting structures of compounds **4**, **7**−**12**, **14**, and **16** in Schemes 2, 3, and 4 were generated by GaussView 3.0 software and then fully optimized without any symmetry restrictions at the B3LYP level. The B3LYP functional consists of Becke's three-parameter hybrid exchange functional[42a] combined with the Lee−Yang−Parr correlation function.[42b] A split-valence plus polarization basis set, 6-31G(d), was used. The DFT/B3LYP/6-31G(d)-optimized structures for the model compounds were used for electronic-structure analysis. HOMO and LUMO isosurfaces for each compound were plotted using the Jmol software (http://jmol.sourceforge.net/).

***N*-(4-Trifluoromethylbenzoyl)-*N*′-(2-thiophenecarbonyl)hydrazide.** 2-Thiophenecarboxylic acid hydrazide (4.26 g, 30 mmol) was dissolved in 30 mL of NMP, after which 4.47 mL (6.26 g, 30 mmol) of 4-(trifluoromethyl)benzoyl chloride was added dropwise at room temperature. After the reaction mixture was stirred overnight at that temperature, it was poured into water, and then aqueous sodium bicarbonate was added slowly and carefully. The precipitated white solid was collected by filtration and washed with water. The product was isolated as a white solid in 95% yield (8.95 g, 28.5 mmol) that was sufficiently pure for subsequent use. Mp: 218 °C. ^{1}H NMR (DMSO-d_6, 400 MHz): δ 10.73 (s, 2H, N−*H*), 8.12 (d, 2H, J = 8.4 Hz), 7.91 (d, 2H, J = 8.4 Hz), 7.90 (d, 1H, J = 4.8 Hz), 7.86 (d, 1H, J = 4.8 Hz), 7.21 (dd, 1H, J = 4.8 Hz).

2-(2-Thienyl)-5-(4-trifluoromethylphenyl)-1,3,4-oxadiazole. $POCl_3$ (25 mL) was added to 8.7 g (27.7 mmol) of the hydrazide from the previous step, and the mixture was stirred for 2 h at 110 °C. After the solution was cooled, excess $POCl_3$ was evaporated. The reaction residue was poured into a large amount of stirred water, after which aqueous sodium bicarbonate was added slowly and carefully. The white precipitate was collected by filtration and washed with water. The oven-dried product (7.8 g, 26.3 mmol, 95% yield) was pure enough for further reaction. Mp: 118 °C. ^{1}H NMR ($CDCl_3$, 400 MHz): δ 8.24 (d, 2H, J = 8.0 Hz), 7.86 (d, 1H, J = 4.0 Hz), 7.79 (d, 2H, J = 8.0 Hz), 7.61 (d, 1H, J = 4.0 Hz), 7.22 (dd, 1H, J = 4.0 Hz).

2-(5-Bromo-2-thienyl)-5-(4-trifluoromethylphenyl)-1,3,4-oxadiazole (1). Oxadiazole from the previous step (4.27 g, 14.4 mmol) and NBS (2.57 g, 14.4 mmol) were dissolved in a mixture of 10 mL of dichloromethane and 30 mL of CF_3COOH. Without light, the solution was stirred for 1 day at ambient temperature. After 50 mL of water and same amount of dichloromethane were added, the organic layer was washed twice with water. The collected organic solution was dried with anhydrous $MgSO_4$ and evaporated. The product was recrystallized from EtOH and acquired as an off-white solid (4.2 g, 11.2 mmol, 78% yield). Mp: 123 °C. ^{1}H NMR ($CDCl_3$, 400 MHz): δ 8.23 (d, 2H, J = 8.0 Hz), 7.80 (d, 2H, J = 8.0 Hz), 7.61 (d, 1H, J = 4.0 Hz), 7.18 (d, 1H, J = 4.0 Hz). Anal. Calcd for $C_{13}H_6BrF_3N_2OS$: C, 41.62; H, 1.61; N, 7.47. Found: C, 41.49; H, 1.69; N, 7.97.

***N*-(Perfluoropentanoyl)-*N*′-(2-thiophenecarbonyl)hydrazide.** 2-Thiophenecarboxylic acid hydrazide (1.42 g, 10 mmol) was dissolved in 20 mL of NMP, and then 3.2 mL (5.1 g, 10 mmol) of perfluoropentanoic anhydride was added dropwise at room temperature. The reaction mixture was stirred overnight and poured into water (sodium bicarbonate was NOT used in this procedure). The precipitated white solid was collected by filtration and washed with water. The white product (3.75 g, 9.66 mmol, 96% yield) was pure enough for use in the next step Mp: 105 °C. ^{1}H NMR (DMSO-d_6, 400 MHz): δ 11.68 (s, 1H, N−*H*), 10.87 (s, 1H, N−*H*), 7.89 (d, 1H, J = 4.8 Hz), 7.86 (d, 1H, J = 3.6 Hz), 7.22 (dd, 1H, J = 4.8 Hz, J = 3.6 Hz).

2-(2-Thienyl)-5-(perfluorobutyl)-1,3,4-oxadiazole. $POCl_3$ (15 mL) was added to 4.65 g (13.8 mmol) of the hydrazide from the previous step, and the mixture was stirred for 2 h at 110 °C. The reaction mixture was cooled and then poured onto ice, and the white precipitate was collected by filtration. The raw products were purified by recrystallization from ethanol, giving the product (3.0 g, 8.1 mmol, 72% yield) as white plates. Mp: 53 °C. ^{1}H NMR ($CDCl_3$, 400 MHz): δ 7.92 (d, 1H, J = 3.6 Hz), 7.71 (d, 1H, J = 3.6 Hz), 7.27 (dd, 1H, J = 3.6 Hz).

2-(5-Bromo-2-thienyl)-5-(perfluorobutyl)-1,3,4-oxadiazole (2). Oxadiazole from the previous step (5 g, 13.5 mmol) and NBS (2.4 g, 13.5 mmol) were dissolved in 25 mL of CF_3COOH. Without light, the solution was stirred for 1 day at 70 °C. After the mixture was cooled, 50 mL of water and same amount of hexane were added; the organic layer was then washed twice with water. The collected organic solution was dried with anhydrous $MgSO_4$ and evaporated. The pure product **2** was isolated by silica gel chromatography (with 1:1 ethyl acetate/hexane as the eluent) as a yellow solid in 90% yield (5.5 g, 12.2 mmol). Mp: 58 °C. ^{1}H NMR ($CDCl_3$, 400 MHz): δ 7.63 (d, 1H, J = 4.0 Hz), 7.20 (d, 1H, J = 4.0 Hz). Anal. Calcd for $C_{10}H_2BrF_9N_2OS$: C, 26.74; H, 0.45; N, 6.24. Found: C, 26.39; H, 0.49; N, 6.37.

5,5‴-Bis(5-perfluorobutyl-1,3,4-oxadiazole-2-yl)-2,2′:5′,2″:5″,2‴-quaterthiophene (4). A stirred solution of bromooxadiazole (1.08 g, 2.4 mmol) and 5,5′-bis(trimethylstannyl)-2,2′-bithiophene (0.49 g, 1 mmol) in 30 mL of 1:1 toluene/DMF was degassed with blowing N_2 for 30 min, after which $Pd(PPh_3)_4$ (0.116 g, 0.1 mmol) was added. The reaction mixture was heated at 100 °C for 1 day. After the mixture was cooled, the precipitated red solid was collected by filtration and then washed with ethyl acetate and hot chlorobenzene. The highly insoluble crude product (0.79 g, 0.875 mmol, 88% yield) was dried in an oven and purified by sublimation in vacuum for use in the fabrication. Mp: 292 °C. MALDI-TOF MS: m/z 903 (M^+). Anal. Calcd for $C_{28}H_8F_{18}N_4O_2S_4$: C, 37.26; H, 0.89; N, 6.21. Found: C, 37.08; H, 0.94; N, 6.52.

2,7-Bis(4,4,5,5-tetramethyl-1,3,2-dioxaborolanyl)-9-fluorenone (5). To a previously degassed 1,4-dioxane (25 mL) solution of 2,7-dibromo-9-fluorenone (2.2 g, 6.5 mmol) were added bis(pinacolato)diboron (3.96 g, 15.6 mmol), $PdCl_2$(dppf) (0.28 g, 0.325 mmol), and KOAc (3.19 g, 32.5 mmol), and the mixture was stirred at 100 °C overnight. After the solution was cooled, the dioxane was removed under vacuum, and then CH_2Cl_2 and water were added. The resulting mixture was extracted with dichloromethane (100 mL) twice, and the organic layer was washed with water and brine and then dried over $MgSO_4$. The organic solvent was concentrated in vacuo to yield a dark-black solid. The pure product **5** was isolated by silica gel column chromatography (using as eluents first 1:1 methylene/hexane to remove the starting material and then 1:5 to 1:3 ethyl acetate/hexane) in 80% yield as a yellow solid. Mp: 230 °C. ^{1}H NMR ($CDCl_3$, 400 MHz): δ 8.12 (s, 2H), 7.94 (d, 2H, J = 7.6 Hz), 7.55 (d, 2H, J = 7.6 Hz), 1.34 (s, 24H, C−C*H*$_3$). ^{13}C{^{1}H} NMR ($CDCl_3$, 400 MHz): δ 193.9, 146.8, 141.5, 133.8, 130.6, 128.2, 120.1, 84.3, 25.0. Anal. Calcd for $C_{25}H_{30}B_2O_5$: C, 69.49; H, 7.00. Found: C, 69.25; H, 6.92.

2,3-Bis[4-(4,4,5,5-tetramethyl-1,3,2-dioxaborolan-2-yl)phenyl]fumaronitrile (6). Compound **6** was prepared in 83% yield using the same procedure as described for **5**, except that bis(4-bromophenyl)fumaronitrile was used instead of 2,7-dibromo-9-fluorenone. Mp: 249 °C (dec). ^{1}H NMR ($CDCl_3$, 400 MHz): δ 7.96 (d, 4H, J = 8.0 Hz), 7.82 (d, 4H, J = 8.0 Hz), 1.37 (s, 24H, C−C*H*$_3$). ^{13}C{^{1}H} NMR ($CDCl_3$): δ 135.6, 134.4, 127.9, 126.1, 122.8, 116.6,

(41) Risenstra-Kiracofe, J. C.; Tschumper, G. S.; Schaefer, H. F., III *Chem. Rev.* **2002**, *102*, 231.

(42) (a) Becke, A. D. *Phys. Rev. A* **1988**, *38*, 3098; Becke, A. D. *J. Chem. Phys.* **1993**, *98*, 5648. (b) Lee, C.; Yang, W.; Parr, R. G. *Phys. Rev. B* **1988**, *37*, 785.

84.4, 25.0. Anal. Calcd for $C_{28}H_{32}B_2N_2O_4$: C, 69.74; H, 6.69. Found: C, 69.82; H, 6.60.

2,7-Bis{5-[5-(4-trifluoromethylphenyl)-1,3,4-oxadiazol-2-yl]thiophen-2-yl}-9-fluorenone (7). Compounds **5** (0.432 g, 1 mmol) and **1** (0.9 g, 2.4 mmol) were dissolved in 20 mL of toluene. After aqueous Na_2CO_3 solution (1.0 M, 10 mL) was added to the reaction mixture, N_2 was bubbled for 30 min as a degassing procedure. $Pd(PPh_3)_4$ (0.115 g, 10 mol %) and 2 drops of Aliquat 336 were added to the reaction flask under an inert atmosphere. The mixture was stirred for 24 h at 90 °C. After the mixture was cooled, the precipitated red solid was collected by filtration and then washed with water and toluene several times. The obtained product (0.63 g, 0.82 mmol, 82% yield) was dried in an oven and purified by sublimation to give a bright-red solid. Mp: 335 °C. MALDI-TOF MS: *m*/*z* 769 (M^+). Anal. Calcd for $C_{39}H_{18}F_6N_4O_3S_2$: C, 60.94; H, 2.36; N, 7.29. Found: C, 60.81; H, 2.32; N, 7.42.

2,7-Bis[5-(5-perfluorobutyl-1,3,4-oxadiazol-2-yl)thiophen-2-yl]-9-fluorenone (8). Compound **8** was prepared as a red solid in 75% yield using the same procedure as described for **7**, except that **2** was used instead of **1**. Mp: 314 °C. MALDI-TOF MS: *m*/*z* 916 (M^+). Anal. Calcd for $C_{33}H_{10}F_{18}N_4O_3S_2$: C, 43.24; H, 1.10; N, 6.11. Found: C, 43.01; H, 1.03; N, 5.89.

2,7-Bis(5-perfluorohexylcarbonylthiophen-2-yl)-9-fluorenone (9). Compound **9** was prepared as a red solid in 86% yield using the same procedure as described for **7**, except that **3** was used instead of **1**. Mp: 290 °C. MALDI-TOF MS: *m*/*z* 1037 (M^+). Anal. Calcd for $C_{35}H_{10}F_{26}O_3S_2$: C, 40.56; H, 0.97. Found: C, 40.64; H, 0.87.

Bis{4-[5-(4-trifluoromethylphenyl)-1,3,4-oxadiazol-2-yl]thiophen-2-yl}phenylfumaronitrile (10). Compound **10** was prepared as a yellow solid in 79% yield using the same procedure as described for **7**, except that **6** was used instead of **5**. Mp: 328 °C. MALDI-TOF MS: *m*/*z* 819 (M^+). Anal. Calcd for $C_{42}H_{20}F_6N_6O_2S_2$: C, 61.61; H, 2.46; N, 10.26. Found: C, 61.45; H, 2.56; N, 10.04.

Bis[5-(5-perfluorobutyl-1,3,4-oxadiazol-2-yl)thiophen-2-yl]phenylfumaronitrile (11). Compound **11** was prepared as a yellow solid in 85% yield using the same procedure as described for **8**, except that **6** was used instead of **5**. Mp: 340 °C. MALDI-TOF MS: *m*/*z* 967 (M^+). Anal. Calcd for $C_{36}H_{12}F_{18}N_6O_2S_2$: C, 44.73; H, 1.25; N, 8.69. Found: C, 44.87; H, 1.18; N, 8.69.

Bis[5-(5-perfluorohexylcarbonylthiophen-2-yl)phenyl]fumaronitrile (12). Compound **12** was prepared as a yellow solid in 72% yield using the same procedure as described for **9**, except that **6** was used instead of **5**. Mp: 279 °C. MALDI-TOF MS: *m*/*z* 1086 (M^+). Anal. Calcd for $C_{38}H_{12}F_{26}N_2O_2S_2$: C, 42.00; H, 1.11; N, 2.58. Found: C, 42.03; H, 1.01; N, 2.66.

2,5-Bis[5-(4,4,5,5-tetramethyl-1,3,2-dioxaborolanyl)-2-thienyl]-1,3,4-oxadiazole (13). To a stirred THF solution (70 mL) of 2,5-bis(5-bromo-2-thienyl)-1,3,4-oxadiazole (2.6 g, 6.63 mmol) was added a solution of *n*-BuLi (6.4 mL, 15.9 mmol, 2.5 M in hexane) at −78 °C, and the reaction mixture was stirred for 30 min at that temperature. After a yellow salt was formed, 2-isopropoxy-4,4,5,5-tetramethyl-1,3,2-dioxaborolane (2.72 mL, 2.48 g, 13.3 mmol) was added to this slurry at −78 °C. The reaction mixture was slowly warmed to ambient temperature and stirred for 12 h. The solvent was removed under reduced pressure, and H_2O and CH_2Cl_2 were added to the resulting mixture. Next, the product was extracted with CH_2Cl_2 (75 mL) twice. After evaporation, the pure product **13** was isolated by silica gel column chromatography (1:3 ethyl acetate/hexane as eluent) in 22% yield (0.72 g, 1.48 mmol) as a yellow solid. Mp: 242 °C (dec). ^{1}H NMR ($CDCl_3$, 300 MHz): δ 7.84 (d, 2H, J = 2.7 Hz), 7.64 (d, 2H, J = 2.7 Hz), 1.36 (s, 24H, C−CH_3). Anal. Calcd for $C_{22}H_{28}B_2N_2O_5S_2$: C, 54.34; H, 5.80; N, 5.76. Found: C, 54.15; H, 5.70; N, 5.56.

2,5-Bis[5-(5-perfluorohexylcarbonyl-2-thienyl)-2-thienyl]-1,3,4-oxadiazole (14). Compounds **13** (0.34 g, 0.7 mmol) and **3** (0.78 g, 1.54 mmol) were dissolved in 20 mL of toluene. After aqueous Na_2CO_3 solution (1.0 M, 7 mL) was added to the reaction mixture, N_2 was bubbled for 30 min. A catalytic amount of $Pd(PPh_3)_4$ (0.08 g, 10 mol %) and 2 drops of Aliquat 336 were added to the reaction flask under an inert atmosphere. The mixture was stirred for 24 h at 90 °C and then cooled, after which the precipitated yellow solid was collected by filtration and washed with water and toluene several times. The obtained product (0.56 g, 0.51 mmol, 73% yield) was dried in an oven and purified by sublimation to give a bright-yellow solid. Mp: 250 °C. MALDI-TOF MS: *m*/*z* 1091 (M^+). Anal. Calcd for $C_{32}H_8F_{26}N_2O_3S_4$: C, 35.24; H, 0.74; N, 2.57. Found: C, 34.85; H, 0.85; N, 2.76.

2,5-Bis[4-(4,4,5,5-tetramethyl-1,3,2-dioxaborolanyl)phenyl]-1,3,4-oxadiazole (15). Compound **15** was prepared as a yellow solid in 84% yield using the same procedure as described for **5**, except that 2,5-bis(4-bromophenyl)-1,3,4-oxadiazole was used instead of 2,7-dibromo-9-fluorenone. Mp: 249 °C (dec). ^{1}H NMR ($CDCl_3$, 300 MHz): δ 8.14 (d, 4H, J = 8.4 Hz), 7.96 (d, 4H, J = 8.4 Hz), 1.37 (s, 24H, C−CH_3). Anal. Calcd for $C_{26}H_{32}B_2N_2O_5$: C, 65.86; H, 6.80; N, 5.91. Found: C, 65.65; H, 6.74; N, 5.78.

2,5-Bis[4-(5-perfluorohexylcarbonyl-2-thienyl)phenyl]-1,3,4-oxadiazole (16). Compound **16** was prepared as a yellow solid in 79% yield using the same procedure as described for **14**, except that **15** was used instead of **13**. Mp: 284 °C. MALDI-TOF MS: *m*/*z* 1078 (M^+). Anal. Calcd for $C_{36}H_{12}F_{26}N_2O_3S_2$: C, 40.09; H, 1.12; N, 2.60. Found: C, 40.04; H, 1.06; N, 2.72.

Acknowledgment. We are grateful to the AFOSR (Award FA9550-06-01-0076), the JHU MRSEC (NSF Division of Materials Research), and DOE (Grant 101636 and a subcontract from Los Alamos National Laboratory) for support of this work. T.L. was supported by a Korean Research Foundation Grant funded by the Korean Government (MOEHRD) (KRF-2005-214-C00210). We thank Professor Peter Searson for access to and assistance with AFM instrumentation.

Supporting Information Available: Additional data in CIF format for compound **10**; absorption spectra of **4**, **9**, **10**, **11**, and **14** in CH_2Cl_2; cyclic voltammograms of **9**, **12**, and **16**; DSC thermograms of **4** and **9**; XRD scans of film of **11**; I_D-V_D curves for the n-channel OFET behavior of **12** in air; crystal data and structure refinement parameters for **10**; summary of diffraction-derived *d*-spacings (*d*) and DFT-computed molecular long-axis lengths (*l*) and tilt angles (φ) in semiconducting films; conformation coordinates from the DFT calculations; and complete ref 11a. This material is available free of charge via the Internet at http://pubs.acs.org.

JA807219X